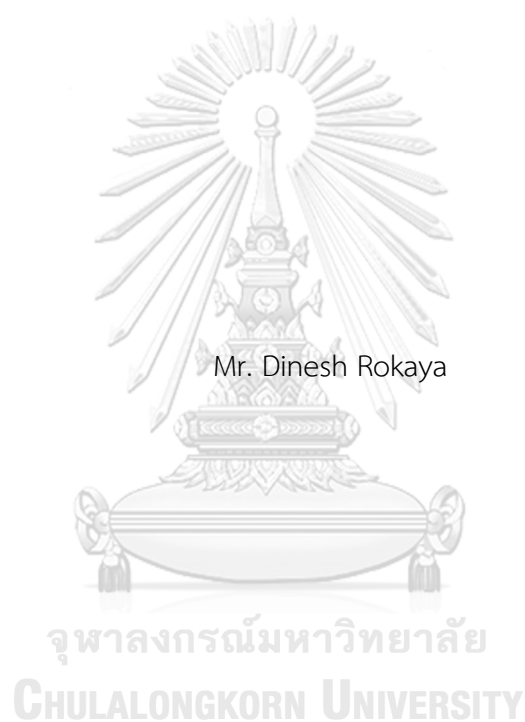


Development of Graphene oxide/Silver Nanocomposite Coating on NiTi Alloy for  
Biomedical Applications



A Dissertation Submitted in Partial Fulfillment of the Requirements  
for the Degree of Doctor of Philosophy in Dental Biomaterials Science  
Inter-Department of Dental Biomaterials Science  
Graduate School  
Chulalongkorn University  
Academic Year 2018  
Copyright of Chulalongkorn University

การพัฒนาการเคลือบโลหะนิกเกิลไททาเนียมด้วยกราฟีนออกไซด์ชีวเวอร์นาโนคอมโพสิตเพื่อการใช้  
งานทางชีวการแพทย์



วิทยานิพนธ์นี้เป็นส่วนหนึ่งของการศึกษาตามหลักสูตรปริญญาวิทยาศาสตรดุษฎีบัณฑิต  
สาขาวิชาทันตชีววัสดุศาสตร์ สหสาขาวิชาทันตชีววัสดุศาสตร์  
บัณฑิตวิทยาลัย จุฬาลงกรณ์มหาวิทยาลัย  
ปีการศึกษา 2561  
ลิขสิทธิ์ของจุฬาลงกรณ์มหาวิทยาลัย



ดิเนช โรคาชา : การพัฒนาการเคลือบโลหะนิกเกิลไททาเนียมด้วยกราฟีนออกไซด์ชีวเวอรรันนาโนคอมโพสิตเพื่อการใช้งานทางชีวการแพทย์. ( Development of Graphene oxide/Silver Nanocomposite Coating on NiTi Alloy for Biomedical Applications) อ.ที่ปรึกษาหลัก : รศ. ดร.วิริทธิ์พล ศรีมณีพงศ์, อ.ที่ปรึกษาร่วม : ดร.เจียเชียน ฉิน, วิไลลักษณ์ ศิริวงศ์รังสรร

การศึกษานี้ ต้องการศึกษาคูณสมบัติทางกล ลักษณะพื้นผิว และทางชีวภาพของโลหะนิกเกิลไททาเนียมที่ได้รับการเคลือบด้วย กราฟีนออกไซด์ชีวเวอรรันนาโนพาทิคิล (GO/Ag) โดยใช้วิธีการเคลือบด้วยวิธี electrostatic deposition ที่ความต่างศักย์ 30 โวลต์ ที่ระยะเวลาต่างกัน 1 5 และ 10 นาที โดยศึกษาลักษณะพื้นผิวด้วย Scanning electron microscope Raman spectroscopy Energy dispersive spectroscopy Surface Profilometer Atomic force microscope รวมถึงศึกษาคูณสมบัติทางกล ได้แก่ยังโมดูลัส ความแข็งผิว ค่าสัมประสิทธิ์ความฝืด โดยการศึกษาที่ใช้ Atomic force microscope ทดสอบการยึดติดของพื้นผิวเคลือบ ส่วนการทดสอบการเข้ากันได้ทางชีวภาพ จะใช้เซลล์ Human gingival fibrous ด้วยวิธี 3-[4,5-dimethylthiazol-2-yl]-2,5-diphenyltetrazolium bromide (MTT) assay ผลการทดสอบจะถูกวิเคราะห์ทางสถิติที่ระดับความเชื่อถือ 0.05 ผลที่ได้เมื่อศึกษาด้วย Raman spectroscopy จะพบว่า D-Band ที่  $1300\text{ cm}^{-1}$  และ G-Band ที่  $1600\text{ cm}^{-1}$  โดยสัดส่วน D และ G Band เท่ากับ 0.83 และพบว่าความหนาของผิวเคลือบด้วย GO อยู่ระหว่าง 0.34 ถึง 1.12 ไมครอน และผิวเคลือบด้วย GO/Ag อยู่ระหว่าง 0.45 ถึง 1.33 ไมครอน โดยพบว่าเมื่อเพิ่มระยะเวลาการเคลือบจาก 1 นาทีเป็น 10 นาที ความหนา ความหยาบ และค่ายังโมดูลัสก็เพิ่มขึ้น ในขณะที่ความแข็งผิวลดลงเมื่อเวลาการเคลือบเพิ่มขึ้น ส่วนค่าสัมประสิทธิ์ความฝืดมีค่าลดลงเมื่อเปรียบเทียบกับโลหะที่ไม่ได้เคลือบ การศึกษานี้แสดงให้เห็นว่าโลหะนิกเกิลไททาเนียมที่ผ่านการเคลือบด้วย GO หรือ GO/Ag มีความแข็งแรงทางกลที่เพิ่มขึ้น แต่มีค่าสัมประสิทธิ์ความฝืดลดลง นอกจากนี้ความเข้ากันได้ทางชีวภาพก็พบว่าโลหะที่เคลือบด้วย GO หรือ GO/Ag จะมีความเข้ากันได้ทางชีวภาพที่ดีขึ้นเมื่อเคลือบเพียงแค่ 1 นาที ดังนั้นโลหะนิกเกิลไททาเนียมที่เคลือบด้วย GO หรือ GO/Ag สามารถนำไปใช้ทางการแพทย์ได้

สาขาวิชา ทันตชีววัสดุศาสตร์

ปีการศึกษา 2561

ลายมือชื่อนิสิต .....

ลายมือชื่อ อ.ที่ปรึกษาหลัก .....

ลายมือชื่อ อ.ที่ปรึกษาร่วม .....

ลายมือชื่อ อ.ที่ปรึกษาร่วม .....

# # 5887821420 : MAJOR DENTAL BIOMATERIALS SCIENCE

KEYWORD: NITI ALLOY, COATING, GRAPHENE OXIDE, SILVER NANOPARTICLES

Dinesh Rokaya : Development of Graphene oxide/Silver Nanocomposite Coating on NiTi Alloy for Biomedical Applications. Advisor: Assoc. Prof. Dr. VIRITPON SRIMANEEPPONG, Ph.D. Co-advisor: Dr. Jiaqian Qin, Ph.D., Asst. Prof. Dr. Vilailuck Siriwongrungsom, Ph.D.

The study aimed to evaluate the surface, mechanical, and biological properties of graphene oxide/silver nanocomposite (GO/Ag) coated NiTi alloy. Substrates were coated using the electrophoretic deposition at 30 V for 1, 5, and 10 min, and were characterized by scanning electron microscope, Raman spectroscopy, energy dispersive spectroscopy, surface profilometer, and atomic force microscope (AFM). Hardness, modulus of elasticity, and friction were done and surface adhesion was measured from AFM. Biocompatibility testing was done on human gingival fibroblasts using 3-[4,5-dimethylthiazol-2-yl]-2, 5-diphenyltetrazolium bromide (MTT) assay. Data were analyzed using SPSS 16; One-way ANOVA with post hoc Scheffe Test ( $P = 0.05$ ). The coatings were confirmed from Raman spectroscopy (D bands at  $\sim 1300 \text{ cm}^{-1}$ , G bands at  $\sim 1600 \text{ cm}^{-1}$  and ratio of D and G band was 0.83). The thickness of the coatings ranged from 0.34 to 1.12  $\mu\text{m}$  for the GO and 0.45 to 1.33  $\mu\text{m}$  for the GO/Ag coatings. Increasing coating time increased the roughness, thickness, and Young's modulus but decreased the hardness. The friction of the coated alloy was lower than the uncoated alloy. Uncoated NiTi group showed less viable cells than the coated and control group. 10 min coatings showed higher viable cells than 1 and 5 min. The GO and the GO/Ag-coated NiTi alloys can be used for biomedical applications.

Field of Study: Dental Biomaterials  
Science

Student's Signature .....

Academic Year: 2018

Advisor's Signature .....

Co-advisor's Signature .....

Co-advisor's Signature .....

## ACKNOWLEDGEMENTS

First of all, I would thank my thesis major advisor Associate Professor Dr. Viritpon Srimaneepong whose continuous guidance, support and persistent encouragement helped through my qualification examination, PhD research work, and publication of manuscripts. I am very grateful to my co-advisor Dr. Jiaqian Qin for the continuous support for the conduction of PhD research work and publication of manuscripts and Prof. Dr. Pasutha Thunyakitpisal the guidance for cell culture works, advice and encouragements.

In addition, I am grateful to Assistant Professor Vilailuck Siriwongrungson and Dr. Kritsana Siraleartmukul for their support and valuable guidance from initial advice and contacts in the early stages of conceptual research design. I would like to thank the chair of my thesis defense for her time and fulfilling information.

I would also like to acknowledge Chulalongkorn University for granting me “the 100th Anniversary Chulalongkorn University Fund for Doctoral Scholarship” and Ratchadapisek Sompote Fund and Ratchadapisek Sompote Endowment Fund granted to the Surface Coatings Technology for the Metals and Materials Research Unit. I would also like to thank Horiba Scientific Inc. and Puditec Co., Ltd. for their support of the Raman spectroscopy and atomic force microscopy, respectively. I would like to express my greatest gratitude to the staffs of Dental Biomaterials Science programs and PhD students who have helped and supported me throughout my research projects.

Finally, I wish to thank my family for their undivided support, understanding, and encouragement.

Dinesh Rokaya

## TABLE OF CONTENTS

	Page
ABSTRACT (THAI) .....	iii
ABSTRACT (ENGLISH) .....	iv
ACKNOWLEDGEMENTS .....	v
TABLE OF CONTENTS .....	vi
LIST OF TABLES .....	xi
LIST OF FIGURES .....	xii
CHAPTER I .....	16
INTRODUCTION .....	16
1.1 Background and Rationale .....	16
1.2 Objectives of this study .....	19
1.3 Research Hypothesis.....	19
1.4 Scope of this Study.....	20
CHAPTER II.....	21
LITERATURE REVIEW .....	21
2.1 Biomaterials .....	21
2.2 Biocompatibility .....	22

2.3 Requirements of Biomaterials .....	22
2.4 Types of Biomaterials.....	24
2.4.1 Metals .....	24
2.4.2 Ceramics.....	26
2.4.3 Polymers .....	27
2.5 NiTi Alloy .....	27
2.6 Graphene.....	34
2.6.1 Mechanical properties of graphene .....	34
2.6.2 Biocompatibility and Biomedical uses of Graphene .....	36
2.6.3 Surface Characterization of Graphene.....	37
2.6.4 Bonding (Adhesion) of Graphene to Metal.....	39
2.6.5 Low Friction of Graphene.....	41
2.7 Surface Modifications of NiTi Alloy .....	42
2.8 Polymeric Coatings on NiTi Alloy .....	42
2.9 Graphene Coatings.....	45
2.10 Silver Coatings.....	46
2.11 Graphene Nanocomposite Coatings.....	47
2.12 Conceptual Framework of this Research .....	49
CHAPTER III.....	50



MATERIALS AND METHODS .....	50
3.1 Overview of this Study.....	50
3.2 Sample Preparation .....	50
3.3 Graphene Oxide (GO) Solution Preparation .....	51
3.4 GO/AgNPs Solution Preparation.....	51
3.5 EPD of GO and GO/AgNPs .....	52
3.6 Surface Characterization of the Coatings .....	53
3.7 Mechanical Properties of the Coatings .....	53
3.7.1 Coating Thickness and Surface Roughness.....	54
3.7.3 Friction Coefficient .....	54
3.7.4 Hardness and Modulus of Elasticity.....	54
3.7.5 Adhesion Force and Energy .....	55
3.8 Biocompatibility of the Coatings .....	55
3.8.1 Cell Culture.....	56
3.8.2 MTT Cytotoxicity Assay.....	57
3.9 Statistical Analysis .....	58
CHAPTER IV .....	59
RESULTS .....	59
4.1 Results of Surface Characterization of NiTi alloy .....	59

4.2 Results of Surface Characterization of the Coatings.....	60
4.2.1 SEM/ EDS.....	60
4.2.2 Surface Profilometry .....	62
4.2.3 Raman Spectroscopy .....	63
4.2.4 Atomic Fluorescopy Microscopy (AFM).....	64
4.3 Results of Coatings Thickness and Surface Roughness.....	67
4.4 Results of Surface Adhesion Properties.....	69
4.5 Results of the Friction Coefficient.....	71
4.6 Results of the Hardness and Modulus of Elasticity the Coatings.....	72
4.7 Results of Biocompatibility Testing.....	73
CHAPTER V.....	77
DISCUSSION .....	77
5.1 Surface Characterization of the Coatings .....	77
5.2 Coatings Thickness and Surface Roughness.....	79
5.3 Friction Coefficient of the Coatings.....	80
5.4 Hardness and Modulus of Elasticity of the Coated NiTi Alloy .....	81
5.5 Surface Adhesion Properties of the Coatings .....	81
5.6 Biocompatibility of the Coatings .....	84
CHAPTER VI.....	86

CONCLUSION.....86

APPENDIX .....87

REFERENCES..... 117

VITA ..... 130



## LIST OF TABLES

	Page
Table 1 Physical and mechanical properties of NiTi alloy [6, 52, 53]. .....	28
Table 2 Biomedical applications of NiTi alloy [6, 52]. .....	30
Table 3 Physical and mechanical properties of graphene [10, 82]. .....	35
Table 4 Different polymer coatings on NiTi alloys for biomedical applications. ....	43
Table 5 Different studies of graphene and GO coatings on various substrates. ....	45
Table 6 Different studies of Ag-coatings on various substrates. ....	46
Table 7 Different studies of graphene nanocomposite coatings on various substrates. .....	48

## LIST OF FIGURES

	Page
Figure 1 Various biomaterial applications of in the human body [33].....	25
Figure 2 Austenite to martensite transformation, shape memory effect and superelastic hysteresis of NiTi alloy application in stent [55].....	29
Figure 3 Biomedical applications of NiTi superelastic and shape memory alloy (vascular stent, intra-aortic balloon pump, self-expandable stent, surgical endoscopic, and orthodontic archwire) [52, 59].....	31
Figure 4 Raman spectra of GO/Ag nanocomposite [90].....	38
Figure 5 Raman spectra showing the D' peaks of different layers of graphene [95]. ..	39
Figure 6 Detachment of a polymer (pyrrole) coating from NiTi alloy [107].....	45
Figure 7 Conceptual framework of the study.....	49
Figure 8 Overview of the experiment details this study.....	50
Figure 9 Surface morphology of the bare NiTi substrates obtained from: (a) SEM/EDS and (b) surface profilometer and (c) AFM.....	59
Figure 10 SEM/ EDS images of the GO-coated NiTi alloy: (a) 1 min, (b) 5 min, and (c) 10 min.....	60
Figure 11 SEM/ EDS images of the GO/Ag-coated NiTi alloy: (a) 1 min, (b) 5 min, and (c) 10 min. Ag ions are marked in each EDS spectrum. Ag ions are marked in the EDS spectrum.....	61

Figure 12 EDS elemental analysis (wt%) of the GO-coated and the GO/Ag-coated NiTi alloy substrates. ....	62
Figure 13 Surface profilometer images of the GO-coated (a, b, c) and the GO/Ag-coated (d, e, f) NiTi alloy substrates for 1 min (a, d), 5 min (b, e), and 10 min (c, f). ..	63
Figure 14 Raman spectra of the GO-coated NiTi alloys of coating time: (a) 1 min, (b) 5 min, and (c) 10 min groups, and the GO/Ag-coated NiTi alloys of coating time: (d) 1 min, (e) 5 min, and (f) 10 min groups. ....	64
Figure 15 AFM images and points for the measurement of adhesion force and energy using the contact-mode AFM with CONTSCR nano tip on the GO-coated NiTi alloy substrates for 1 min: (a) and (b), 5 min: (c) and (d), and 10 min: (e) and (f), respectively. ....	65
Figure 16 AFM images and points for the measurement of adhesion force and energy using the contact-mode AFM with CONTSCR nano tip on the GO/Ag-coated NiTi alloy substrates for 1 min: (a) and (b), 5 min: (c) and (d), and 10 min: (e) and (f), respectively. ....	66
Figure 17 Coating thickness of the GO and the GO/Ag coatings on NiTi alloy substrates. * denotes the significant different from GO5 ( $P = 0.005$ ) and GO10 ( $P < 0.001$ ). # denotes significant different from GO1 ( $P = 0.005$ ) and GO10 ( $P < 0.001$ ). $\alpha$ denotes significant different from GO5 ( $P = 0.045$ ) and GOAg10 ( $P < 0.005$ ). $\S$ denotes significant different ( $P < 0.05$ ) from GOAg10 ( $P < 0.001$ ). ....	67
Figure 18 Surface roughness of the bare NiTi, the GO and the GO/Ag coatings on NiTi alloy substrates. * denotes significant different ( $P < 0.001$ ) from GO-coated (GO1, GO5, GO10) and GO/Ag coated (GOAg1, GOAg5, GOAg10). # denotes significant different ( $P < 0.001$ ) from GO5, GO10 and bare NiTi. $\alpha$ denotes significant different ( $P < 0.001$ ) from GO1 and bare NiTi. $\S$ denotes significant different ( $P < 0.001$ ) from GOAg5, GOAg10 and bare NiTi. $\dagger$ denotes significant different ( $P < 0.001$ ) from GOAg1 and bare NiTi. ....	68

Figure 19 Surface adhesion force measured from AFM of the GO-coated and the GO/Ag-coated NiTi alloy substrates. \* denotes significant different ( $P < 0.05$ ) from GO5 and GO10.  $\alpha$  denotes the significant different ( $P < 0.05$ ) from GO1 and GO10. # denotes significant different ( $P < 0.05$ ) from GOAg5 and GOAg10. § denotes the significant different ( $P < 0.05$ ) from GOAg1 and GOAg10. ....69

Figure 20 Surface adhesion energy measured from AFM of the GO-coated and the GO/Ag-coated NiTi alloy substrates. \* denotes significant different ( $P < 0.05$ ) from GO5 and GO10.  $\alpha$  denotes the significant different ( $P < 0.05$ ) from GO1 and GO10. # denotes significant different ( $P < 0.05$ ) from GOAg5 and GOAg10. § denotes the significant different ( $P < 0.05$ ) from GOAg5 ( $P < 0.05$ ).....70

Figure 21 Friction coefficient of the bare, the GO-coated and the GO/Ag-coated NiTi alloy substrates. \* denotes significant different ( $P < 0.001$ ) from GO-coated (GO1, GO5, GO10) and GO/Ag coated (GOAg1, GOAg5, GOAg10). # denotes the significant difference ( $P > 0.05$ ) from GO10. § denotes the significant difference ( $P < 0.05$ ) from GOAg10. ....71

Figure 22 Berkovich hardness of the GO-coated and the GO/Ag-coated NiTi alloy substrates of coating time. \* denotes the significant difference ( $P < 0.001$ ) from GO5 and GO10. # denotes significant difference ( $P < 0.001$ ) from GOAg5 and GOAg10. ....72

Figure 23 Modulus of elasticity of the GO-coated and the GO/Ag-coated NiTi alloy substrates of coating time. \* denotes the significant difference ( $P < 0.001$ ) from GO5 and GO10. # denotes significant difference ( $P < 0.001$ ) from GOAg5 and GOAg10. ....73

Figure 24 Microscopy images (20x) of cells (gingival fibroblasts) while seeding of cells of the bare NiTi alloy, the GO-coated (GO1, GO5, GO10), and the GO/Ag-coated (GOAg1, GOAg5, GOAg10) NiTi alloy substrates.....74

Figure 25 Microscopy images (20x) of cells (gingival fibroblasts) after incubating 24 h with conditioned medium of the bare NiTi alloy, the GO-coated (GO1, GO5, GO10), and the GO/Ag-coated (GOAg1, GOAg5, GOAg10) NiTi alloy substrates. ....74

Figure 26 Number of viable cells (gingival fibroblasts) after incubating 24 h in conditioned medium of the bare NiTi alloy, the GO-coated (GO1, GO5, GO10), and the GO/Ag-coated (GOAg1, GOAg5, GOAg10) NiTi alloy substrates and the control (cells incubated with growth medium). The data were obtained from three independent experiments and shown as mean  $\pm$  SD. \* denotes significant different ( $P < 0.001$ ) from GO-coated (GO1, GO5, GO10), the GO/Ag coated (GOAg1, GOAg5, GOAg10) and the control. § denotes the significant difference compared to the GO1 and bare NiTi alloy ( $P < 0.05$ ). α denotes the significant difference compared to the GOAg1 and bare NiTi alloy ( $P < 0.05$ ). # denotes the significant difference compared to the GO1, GO5, GOAg1, GOAg5 and bare NiTi alloy ( $P < 0.05$ )..... 75





# CHAPTER I

## INTRODUCTION

### 1.1 Background and Rationale

Although the use of biomaterials have a long history, the need for safe, useful and suitable materials is increasing in medical field due to the increasing longevity of people's life and high functional and esthetic demands [1]. A biomaterial used in a body made from biocompatible material that is used for medical devices is anticipated to interact with integrative biology in order to access, treat, enhance or replace an organ or function of the body [2].

Majority of the materials used in biomedical applications in the human body are made from metals. Commonly used metallic biomaterials are commercially titanium (Ti) and its alloys, such as nickel-titanium (NiTi), stainless steel (SS), cobalt-chrome (Co-Cr), ceramics, gold based materials, dental amalgam [3, 4].

NiTi alloy is the most elastic and biocompatible alloy compared with other Ni alloys [5]. NiTi alloy fully recovers from 8% deformation strain compared to SS, which recovers only from less than 1% deformation [6]. Common biomedical applications of

NiTi alloys include vascular stents, staples, catheter guide wires, bone fracture fixtures, orthodontic wires, and endodontic files and reamers.

Although there are numerous biomaterials with suitable bulk properties still it is difficult to find an ideal material with excellent surface properties with truly biocompatible for applications in clinics. A biocompatible modified layer with possesses suitable mechanical properties is added to alleviate the above problems. Furthermore, the mechanical properties of materials are determined by the bulk properties, and the tissue biomaterial interactions are determined by the surface properties. These interactions would occur by a very thin layer ( $<1 \mu\text{m}$ ) on the biomaterial [7]. The mechanical and tribological behavior of biomedical devices is rarely investigated. Friction between wires and brackets in orthodontics causes a reduction in the forces that are applied for tooth movement, prolonging the treatment duration [8]. Similarly, the friction and wear properties of biomaterials can result in hemolysis and thrombus formation in blood vessels or biomaterial/medical device failure [9].

Graphene is a thin sheet of  $\text{sp}^2$  carbon atoms that creates a 2-dimensional (2D) hexagonal honeycomb structure [10]. Graphene oxide (GO) is typically prepared by oxidizing graphite using Hummers' method [11]. The GO carbon atoms have oxidized functional hydroxyl, epoxy, and carboxylic acid groups [12]. These functional groups on GO produce diverse compounds with improved physical, mechanical, and biological

properties [13-17]. Graphene and GO is an attractive choice for fabricating various nanocomposites with different polymer matrixes because of its excellent properties such as good biocompatibility, strength, and good stability [10, 18-20]. In addition, the lubrication and friction reduction effects of graphene-based coatings have wide potential for biomedical uses such as orthodontic wires, prostheses, vascular stents, staples, and catheter guide wires [9, 21]. GO and reduced GO have demonstrated antibacterial effects against *S. aureus* and *E. coli* [22]. However, Das *et al.*[23] found no antibacterial effects of GO against *E. coli* and *P. aeruginosa*. These conflicting results have led to the use of other antibacterial agent surface coatings.

Similarly, silver nanoparticles (AgNPs) are strong antibacterial agents with great potential as a surface coating which improves the properties of biomaterials in addition to other uses of AgNPs [24]. Ag composite coatings are antibacterial against both Gram+ and Gram- strains, including *S. aureus* and *E. coli*, whereas they are non-cytotoxic to adipose stem cells, human fibroblasts, and osteoblasts-like cells [25].

Electrodeposition (EPD) is a cost-effective surface coating technique that produces a thin uniform coating with excellent mechanical properties [26-28]. Under an electric field, the charged particles in solution migrate and deposit on the metallic substrate. EPD is a biomaterial and bioactive coating processing technique. Graphene based coatings can be fabricated using EPD for various uses [21, 27, 29-31].

It is necessary improve surface properties of a biomaterials using a biocompatible coating. Thus, the aim of our research was to produce a graphene oxide/silver (GO/Ag) nanocomposite coating on NiTi alloy using EPD to improve surface, mechanical and biological properties for biomedical applications. We hypothesized that GO/Ag nanocomposite coatings on NiTi substrates would improve their mechanical and tribological properties.

## 1.2 Objectives of this study

The main objectives of our research are:

- 1) To develop GO coating on NiTi alloy.
- 2) To develop GO/Ag nanocomposite coating on NiTi alloy.
- 3) To study the surface, mechanical properties, and biocompatibility of GO and GO/Ag nanocomposite coated NiTi alloy.

จุฬาลงกรณ์มหาวิทยาลัย  
CHULALONGKORN UNIVERSITY

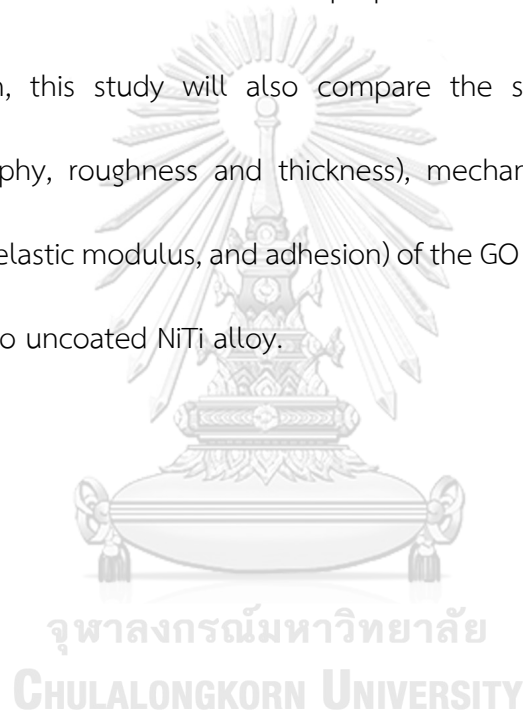
## 1.3 Research Hypothesis

There are no significant differences of the surface, mechanical properties, and the biocompatibility of GO and GO/Ag nanocomposite coating between uncoated and coated NiTi alloy.

#### 1.4 Scope of this Study

Although, Ti and its alloys are considered as the most biocompatible metallic materials are used widespread in medical devices in human body, these materials have side effects Ni toxicity and sensitization. This study will develop the GO and GO/Ag nanocomposite coating on NiTi alloy which will can be implemented in medicine and dentistry for better surface and mechanical properties.

In addition, this study will also compare the surface properties (surface structure, topography, roughness and thickness), mechanical properties (wear and friction, hardness, elastic modulus, and adhesion) of the GO and GO/Ag nanocomposite coated NiTi alloy to uncoated NiTi alloy.



## CHAPTER II

### LITERATURE REVIEW

#### 2.1 Biomaterials

At present, due to the advancements in material science, it has assumed greater significance in various aspects in medicine (dentistry, orthopedics, surgery, ophthalmology, immunology, histopathology) and veterinary. Improvements are being made in the field of dental materials science which suggest that intriguing changes are occurring in the clinical practice of dentistry and medicine. Various medical device and implants are used to diagnose disease/ conditions, to treat, or to prevent, or to affect the structure or any function of the body [32, 33]. Therefore, it is necessary to know the benefits and limitations of these biomaterials before their selection in clinical practice.

Dental biomaterial is the science which deals with the materials used in dentistry, their physical, chemical and mechanical properties, their manipulation and uses. The American Dental Association [34] have evaluated the physiochemical properties of dental biomaterials, instruments and test methods to formulate standards or specification for dental materials and to certify the products which meet those requirements [35].

## 2.2 Biocompatibility

The concept of biocompatibility is given by Williams [36]. According to him, it is the capacity of a biomaterial to perform its function without creating any undesirable effects (local or systemic) during treatment with positive effects at the cellular or tissue level clinically improving the performance. An inert and biologically stable biomaterials are expected to remain unchanged in the body, such as Ti and its alloys remain [2].

FDA has divided medical devices into 3 classes according to their risks, safety and effectiveness [32].

Class I devices: Low risk and are subjected to the lowest regulatory controls to provide reasonable assurance. These devices have the lowest risk to the patient. For example, dental floss.

- Class II devices: Higher risk than Class I and require greater controls. These devices have the moderate risk. For example, elastic bandages.
- Class III devices: Have the highest risk and require the highest level of control.

These devices have the highest risk. For example, replacement heart valves

## 2.3 Requirements of Biomaterials

The important requirement of the biomaterial is its acceptability by the human body. The success of a biomaterial depends on three major factors:

- A. Biological and biocompatibility,
- B. Physical and mechanical properties,

- C. Health state of the recipient, and
- D. Competency of the surgeon.

Firstly, there should not be any adverse effects like inflammation, allergy, carcinogenicity and toxicity from the biomaterial. Secondly, it should have adequate mechanical properties; mechanical strength to withstand the forces under varying loading conditions, wear resistance in corrosive human body environment. Thirdly, biomaterial should not cause any adverse effect on the recipient. In addition, a biomaterial should remain intact for required time period without failure, i.e. 15-20 years in older patients and >20 years for younger patients in implanted biomaterials. In certain cases, biomaterials that are placed for certain period only for example in drug delivery and in orthodontics, it should not be stable for the required duration without adverse effects.

Biomaterials are selected based on above criteria although function the biomaterials are still found to deteriorate and fail over the period of about 12-15 years. In such cases, a revision surgery or new biomaterial is needed in order to regain the functionality of the system [33]. The main concern in selecting material metals for biomedical applications are biocompatibility, appropriate mechanical properties, and the cost. The reasons for their failure are manifold which includes mechanical, chemical, biological, surgical, manufacturing and biocompatibility issues. Elements such as Ni, Co and Cr are found to be released from their respective alloys due to the



corrosion in the body environment [37]. Thus, the surface modification and coatings of these materials have been applied and developed which will be discussed later.

## 2.4 Types of Biomaterials

Broadly, biomaterials used in human body can be broadly classified as: (1) metals, (2) ceramics and (3) polymers as described follows [38]:

### 2.4.1 Metals

Metallic biomaterials are mainly used for the load bearing implants in body due to their superior mechanical properties [1]. High strength can be provided metal alloys. Their applications include implant devices, such as hip joint prostheses, knee joint prostheses, dental implants, cardiovascular devices, surgical instruments, etc as shown in Figure 1 [33].

Majority of the materials used in biomedical applications in the human body are made from metals [e.g. Commercially pure Titanium (CP-Ti) and its alloys, stainless steel (SS), cobalt-chrome (Co-Cr) alloys, nickel-chrome (Ni-Cr)], ceramics [Aluminum oxide ( $Al_2O_3$ ), Zirconia (Zr), Calcium phosphates (CaP)], gold based materials, dental amalgam and synthetic and natural polymers [3, 4].

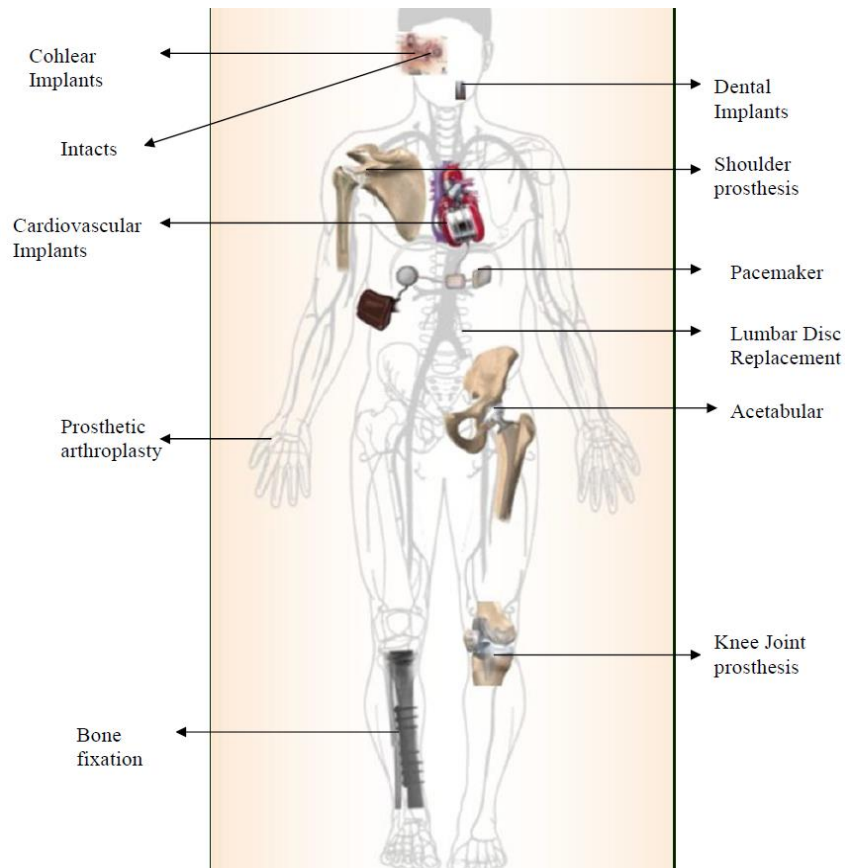


Figure 1 Various biomaterial applications of in the human body [33].

Metal alloys can be of (a) noble (precious) metals such as gold (Au), palladium (Pd), and silver (Ag), and (b) non-precious metal alloys which include SS, Co-Cr, and Ti alloys. High strength metallic biomaterials are made from non-precious metal alloys, and less often precious metals. Alloys of precious metals are usually employed because of their biocompatibility and castability, as compared to those of non-precious metals.

A variety of metallic dental devices includes inlays, crowns, bridges, clasps, dentures, dental implants composed of a fixture and an abutment, and fixed braces.

In dentistry, both precious and non-precious metal alloys are used [39]. Biomaterials for dental applications require a stable due to the variation of the temperature and pH in the oral environment.

#### 2.4.2 Ceramics

Bioceramics have been extensively employed in dentistry and orthopedics [40]. Nowadays, these materials are employed in numerous applications including crowns, cements, dentures, coatings on metal implants, heart valve, and carriers for drug delivery [41]. According to their biological response, bioceramics can be categorized into 3 groups: bioinert (carbon, alumina, zirconia ceramics), bioactive [hydroxyapatite (HA), bioactive glasses, glass ceramics], and bioresorbable (tricalcium phosphate, calcium aluminate) [41]. HA is a representative of calcium phosphate-based bioceramics which is widely used for biomedical applications [41]. Bioinert ceramics are much less applied in orthopedics as they lead to the non-adherent fibrous capsule around the implant, whereas bioactive ceramics in various forms (bulk, coatings, powder, and porous) are universally adopted as orthopedic materials to trigger a chemical bonding with living tissue, which permits not only a mechanical but also biological fixation and thereby avoids implant failure consequences [42]. Ceramics used in dentistry are mostly based on silicon, and usually in the form of silica or various silicates [41, 43].

### 2.4.3 Polymers

Polymers are macromolecules with high molecular mass [44]. Polymers are gaining popular in various fields of medical science. They are widely used in surgery, prosthetic systems and drug delivery. At present, special polymers; shape memory polymers have been used increasingly [45-47].

Polymers can be natural, semisynthetic or synthetic [48]. Polymers are formed by chemical reactions in which large number of monomers which are joined sequentially forming a chain. Mostly, polymers use only one monomer but some may use more than 2 different monomers [48]. Graphene is a kind of polymeric material.

### 2.5 NiTi Alloy

Ti and its alloys are considered as the most biocompatible metallic materials [49, 50]. CP-Ti has various degrees of purity (graded from 1 to 4) which is characterized by oxygen, carbon and iron content. Other elements are added to increase the tensile strength and to reduce its ductility [51]. The NiTi alloys used in medicine and dentistry mostly contain approximately 56% (by wt) Ni and 44% (by wt) Ti. Their properties include great tensile strength, high strength to weight ratio, flexibility, machinability, formability, and apparent biocompatibility are shown in Table 1 and their properties

can be varied according to the composition and thermomechanical processing techniques [4, 6, 36, 52].

Table 1 Physical and mechanical properties of NiTi alloy [6, 52, 53].

Properties		Value
Physical Properties	Density	6.45 gm/cm <sup>3</sup>
	Melting point	1310 °C
	Latent heat of transformation	11.0 x10 <sup>6</sup> /°C
	Thermal conductivity	23.26 kJ/kg
	Electrical resistivity	100 x 10 <sup>-6</sup> Ω-cm
	Hardness 950 °C (Furnace cooled)	89 HRB
	Hardness 950 °C (Quenched-R.T. water)	89 HRB
Mechanical Properties	Young's modulus	120 GPa
	Yield strength	379 MPa
	Ultimate tensile strength	690 – 1380 MPa
	Poisson's ratio	0.33
	Elongation	13 – 40%
	Shape memory recoverable strain	6.5 – 8.5 %
	Super-elastic recoverable strain	up to 8 %
	Hysteresis	30 – 50 °C
	Transformation strain	
	<ul style="list-style-type: none"> <li>● for a single cycle</li> <li>● for 100 cycles</li> <li>● for 100,000 cycles</li> </ul>	<p>maximum 8%</p> <p>6 %</p> <p>4 %</p>

Ti is an allotropic material and exists as a hexagonal close-packed structure (hcp,  $\alpha$ -Ti) till 882 °C and above this temperature it behaves as body-centered cubic structure (bcc,  $\beta$ -Ti). Addition of alloying elements to Ti enables it to have a broad

range of types, including  $\alpha$ -type,  $\beta$ -type and  $\alpha+\beta$ -type alloys [54]. They have an ability to alter their atomic bonding which causes unique and significant changes in the mechanical properties and crystallographic arrangement of the alloy. These changes occur under the changes of temperature and stress. The austenite phase is a stable, body-centered cubic lattice structure of NiTi alloy at high temperature (100 °C). There is martensitic transformation while change in pressure and temperature (Figure 2).

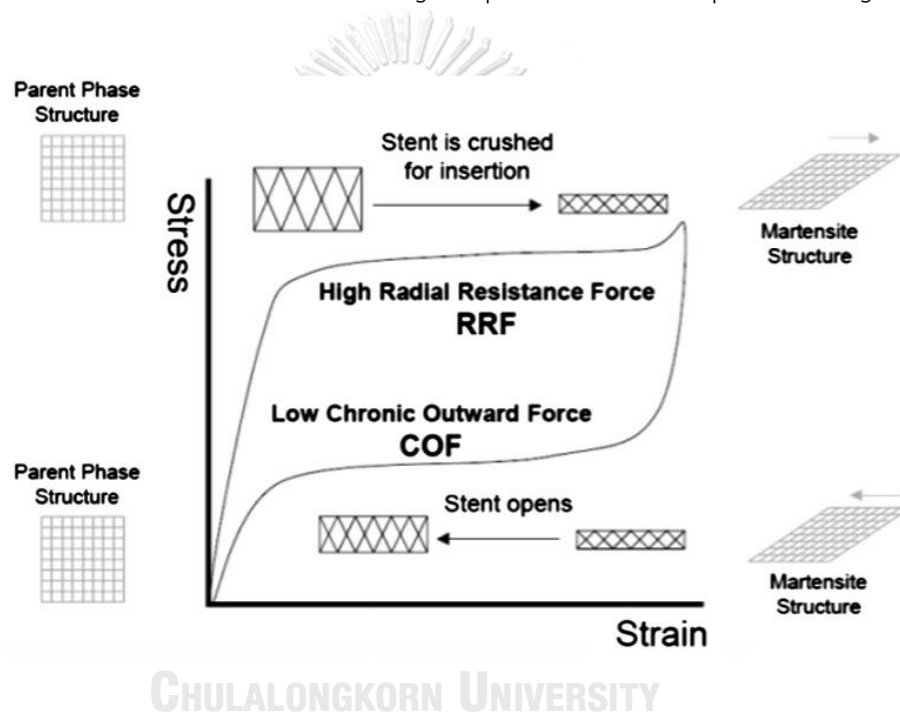


Figure 2 Austenite to martensite transformation, shape memory effect and superelastic hysteresis of NiTi alloy application in stent [55].

These transformation result in changes in the physical properties of the alloy; shape memory effect [56] and super-elasticity [55, 57]. These two unique features are of relevance to medicine [6]. These properties of NiTi alloys are mainly used for various purposed in medicine and dental applications, such as in making intravascular stents,

catheter guide wire, bone fracture fixtures and staples for healing small bone fractures, orthodontic archwires, endodontic reamers and files (Table 2 and Figure 3) [4, 6, 52].

Cardiac stent, an expandable metal mesh device, is used to treat narrowed or blocked coronary arteries. The combination of angioplasty and stent can save a life, especially when performed immediately after a heart attack. The stents are widely used in the management of gastrointestinal obstruction as they provide significantly lower morbidity and mortality rates than surgical alternatives [58].

*Table 2 Biomedical applications of NiTi alloy [6, 52].*

<b>Applications</b>	<b>Shape memory and Superelastic Effects</b>
<b>Vascular applications</b>	Venous filters, devices for closing ventricular septal defects, self-expandable vascular stents, stent-graft, and percutaneous devices to treat valvular diseases
<b>Orthopedic applications</b>	Intraspinal implants, intramedullary nails, staples or plates, devices for correcting scoliosis, spinal vertebrae spacer, intramedullary nails and devices for physiotherapy
<b>Surgical applications</b>	Coils, stents, microguide wires and surgical instruments
<b>Dental applications</b>	Arch wires, endodontic files and tooth distractors.

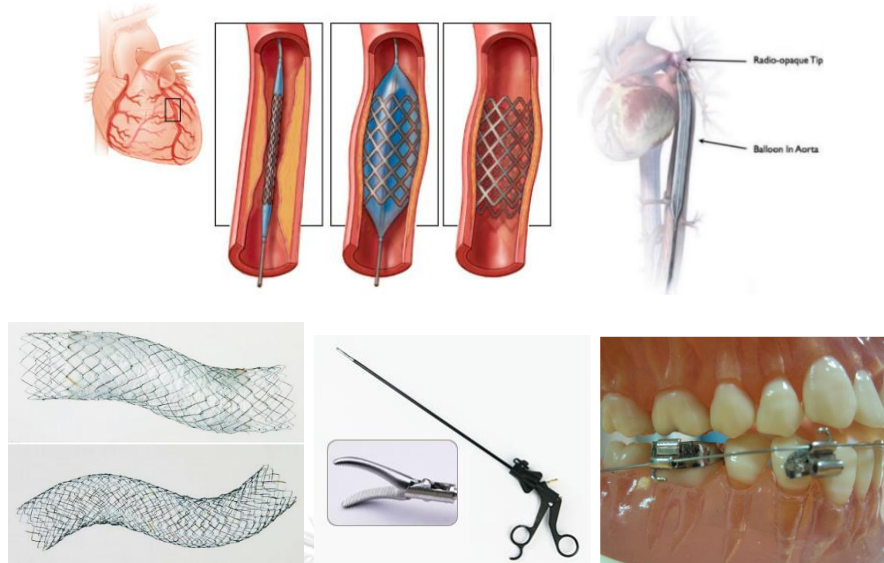


*Figure 3 Biomedical applications of NiTi superelastic and shape memory alloy (vascular stent, intra-aortic balloon pump, self-expandable stent, surgical endoscopic, and orthodontic archwire) [52, 59].*

Patients may experience an allergic reaction to the medications or materials used for angioplasty and stenting. Angioplasty may also cause bleeding, damage to your blood vessel or heart, or irregular heartbeat [60]. Other rare potential complications include heart attack, kidney failure, and stroke. Following insertion and removal of the stent, a scar tissue can form. If that happens, a second procedure may be needed. There's also a risk of blood clots forming within your stent. Studies strongly suggest that the metallic alloy used has a direct impact on the extent of neointima/restenosis formation [60]. Thus, metallic alloys differ not only with respect to mechanical features, but also by their biocompatible properties. These two factors are of major importance in the induction of vessel wall injury, inflammatory processes and cell proliferation. A biocompatible layer is added to alleviate the above problems.



Furthermore, the mechanical properties of biomaterials are dictated by the bulk properties, whereas, the tissue biomaterial interactions are governed by surface properties [7]. Ti has very high attraction for the oxygen and it forms an oxide film spontaneously [61]. Usually, the composition of the protective oxide film is based on TiO, TiO<sub>2</sub>, or Ti<sub>2</sub>O<sub>3</sub> [49, 62]. Ti and its alloys in vivo environments is actually have ability to form a stable, adherent protective oxide layer on their surface [62, 63]. Although the oxide layer is thermodynamically stable, metal ions is still being released through a passive-dissolution mechanism. Hence, the main disadvantage of NiTi alloys is the release of potentially toxic ions of aluminum (Al), vanadium (V), Ni and Ti and can cause cytotoxicity [64]. Two factors play role in the release of metal ions: thin oxide layer (0.1-10 μm) and the protective oxide layer is not superelastic and tendency to crack under strains [4].

It is found that NiTi alloy exhibited pitting type attack compared to compared with SS, Co-Cr and β-Ti [65]. The Ni released from NiTi and stainless steel orthodontic wires, known as allergen, causes the oral signs and symptoms such as; gingival hyperplasia, stomatitis, angular cheilitis, perioral rash, erythema multiforme, burning sensation, and loss of taste [66, 67].

Another important property of devices used in medicine and dentistry is the frictional force generated during various biomaterials used in the body, such as while using stents and in orthodontic mechanotherapy. Generally, it has become an

accepted principle in orthodontics that light continuous forces are desirable to achieve physiologic and controlled tooth movement with minimum pathologic repercussions on the teeth and their surrounding tissues. Orthodontic archwires that can deliver such light forces over long distances would appear to be most useful to clinical professionals during the initial alignment phase of fixed appliance treatment [68]. Bravo *et al.* [69] compared friction test of coated vs uncoated NiTi wires. Frictional tests performed on the archwires under scrutiny on the two different types of brackets (316L stainless steel and the Ti6-Al-4V alloy) provided the values for the static and dynamic friction coefficients. It can be observed that the polymer static and dynamic friction coefficients are lower than  $\beta$ -Ti and CP-Ti, NiTi and NiTiCu orthodontic archwires in both bracket materials tested. The results showed that, the wear rate of polymeric wires is much lower than metallic wires. This contribution evaluated static as well as dynamic friction, and the results indicated a lower friction at the archwire-bracket interface when a polymer and Ti-6Al-4V or 316L stainless steel are used in comparison with the other 4 alloy archwires. Clinically, this means that the net force required for translator movement will be lower for polymer and higher when Ti-based and superelastic alloys (NiTi and NiTiCu) wires are used [70].

## 2.6 Graphene

Graphene has been described as the “thinnest material in the universe”, has attracted attention in various fields including dentistry because it has dramatically improved mechanical properties [71, 72]. Graphene, discovered in 2004 [73], is a carbon nanofiller with a one-atom-thick planar sheet of  $sp^2$  bonded carbon atoms that are densely packed in a honeycomb crystal lattice [10, 74]. It can be synthesized by 4 methods: (a) chemical vapour deposition (CVD) such as the decomposition of ethylene on metal surface, (b) micromechanical exfoliation of graphite, (c) epitaxial growth on electrically insulating surfaces, such as SiC, and (d) solution-based reduction of GO [10].

### 2.6.1 Mechanical properties of graphene

Mechanical properties of graphene and GO are mentioned below which includes unique properties [75]:

- Mechanical stiffness,
- Very high mechanical strength,
- Very high electrical and thermal conductivity,
- Optical properties,
- Elasticity and can serve as a solid or colloidal lubricant.
- Unique friction and wear properties, and
- Hydrophobic and stable in polar solvents (with addition of surfactant).

GO is a oxygen-containing graphene [76]. Both for graphene and GO indicates the presence of oxygen on the surface of the protected steel surface (28 % for graphene flakes and 43% for GO layers) [77]. Reduced GO (rGO) is the reduction derivative of GO, although the electrical, thermal, mechanical properties and surface morphology of RGO and pristine graphene are similar [78]. GO reduction is a process that converts  $sp^3$  carbon to  $sp^2$  carbon. Various agents to reduce GO to rGO includes hydrazine hydrate, dimethyl-hydrazine, hydroquinone and sodium tetrahydridoborate [78].

Various methods used for graphene coating are CVD [79, 80], electrophoretic deposition (EPD), spin coating, dip coating, layer-by-layer self-assembling, sol-gel process, spray coating and liquid exfoliation [81]. The physical and mechanical properties of graphene GO and reduced GO (rGO) are shown in Table 3.

Table 3 Physical and mechanical properties of graphene [10, 82].

Properties	Graphene	GO	rGO
Electrical Resistivity	$10^{-6} \Omega\text{-cm}$	NA	NA
Thermal conductivity	5000 W/m-K	2000 W/m-K	0.14-0.87 W/mK
Optical Transmission	97.7%	<50%	60–90%
Coefficient of thermal expansion	$-6 \times 10^{-4} / \text{K}$	NA	NA
Electrical conductivity	$10^4 \text{ S/cm}$	$10^{-1} \text{ S/cm}$	200–35,000 S/cm
Young's modulus	1 TPa	0.22 TPa	NA
Tensile strength	130 GPa	120 GPa	NA
Poisson's ratio	0.18	-	-

## 2.6.2 Biocompatibility and Biomedical uses of Graphene

Graphene is a biocompatible biomaterial and used of GO materials in fabricating nanocomposites with different polymer [10, 83]. Graphene is considered as an ideal candidate for implant surface coatings as it is chemically inert, atomically smooth and highly durable. Graphene materials are commonly used in biomedical engineering and biotechnology such as nanoelectronics, sensors, energy technology, and composite materials. The biomedical applications of graphene include biosensing/ bioimaging, drug delivery, cancer photothermal therapy, antibacterial materials, biomedical engineering, biotechnology and regenerative medicine [84].

Graphene can be incorporated with nanoparticles to make antibacterial coating. Nanosilver is also regarded as an antibacterial agent as it has great potential to be utilized in antibacterial surface coatings for dental biomaterials. Recently, polymers have been employed to fabricate nanocomposite coatings with nanosilver for better properties with enhanced antibacterial activity [25]. In addition, silver nanoparticles (AgNPs) were deposited onto the functionalized hybrid graphene. shows better antimicrobial activity both against Gram+ *S. aureus* and Gram- *E. coli* at lower concentration compared to without applying AgNPs. Such biocompatible antimicrobial polymeric films of graphene have good potential for various dental biomaterial, such as prosthesis, archwires and endodontic files.

### 2.6.3 Surface Characterization of Graphene

The commonly used method to study the surface characteristics of the graphene oxide coatings on NiTi alloy methods are: Scanning electronic microscope (SEM), transmission electron microscopy (TEM), Energy dispersive spectroscopy (EDS), Surface profilometer, Raman spectroscopy, Atomic force microscopy (AFM), and X-ray diffraction (XRD) [85]. SEM and TEM is used to study the surface microstructure. In addition, transmission electron microscopy. Surface profilometer can be used to determine the thickness of GO. It also helps to measure the mean roughness ( $R_a$ ) and maximum roughness depth ( $R_{max}$ ) of the irregularities of the GO coating NiTi alloy [85].

Raman spectra is a useful for studying carbon structure. The Raman spectrum of graphene shows a distinct D band at approx.  $1,300\text{ cm}^{-1}$  and a G band at approx.  $1,600\text{ cm}^{-1}$  [86, 87]. The D band represents edges, other defects, disordered carbon due to the vibration of  $sp^3$  bonded carbon atoms, and impurities. The G band represents the zone center  $E^{2g}$  mode, corresponding to ordered  $sp^2$  bonded carbon atoms [78]. Singh et al. [86] found the ratio of D band and G bands ( $I_D/I_G$ ) of GO composite coating to be 0.85 (D and G bands at  $1353\text{ cm}^{-1}$  and  $1591\text{ cm}^{-1}$ , respectively), whereas, of rGO composite coating to be 0.937 (D and G bands at  $1353\text{ cm}^{-1}$  and  $1584\text{ cm}^{-1}$ , respectively). The Raman spectra of the graphene/Ag nanocomposite, D and G bands, and  $I_D/I_G$  is slightly increased [88]. The increase may be related to an increase in the degree of disorder of the GO matrix, in part due to chemical bonds between

the GO matrix and Ag nanoparticles [88]. The presence of AgNPs in the GO nanocomposite can be also confirmed from EDS and XRD. AFM allows to observe molecular and atomic level features. The surface roughness ( $R_a$ ) can be also studied from surface profilometer or AFM. EDS helps to investigate the elemental analysis, such as carbon (C), oxygen (O), and elements, such as Ni, Ti in GO and Ag, in GO/Ag nanocomposite [89].

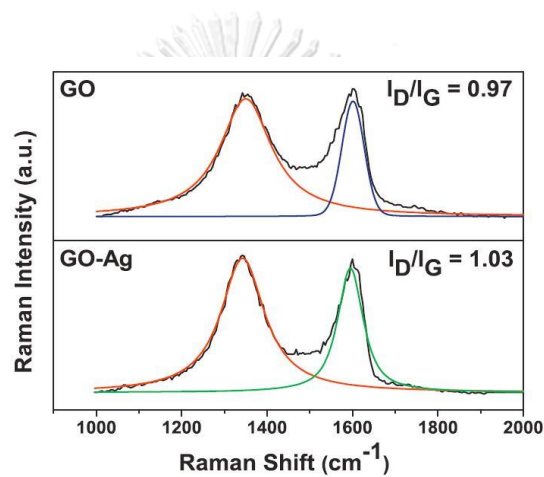


Figure 4 Raman spectra of GO/Ag nanocomposite [90].

The thickness of a single layer graphene is found to be 0.35 nm [91]. Few-layer graphene is a few atomic-layer-thick material with interlayer spacing of 0.34 nm, and it exhibits substrate dependent properties of electronic, photonic, thermal and photoelectric properties [92]. A number of techniques to determine the thickness of graphene films includes optical contrast, Raman scattering and scanning probe microscopy [93]. An AFM can be used to identify the number of graphene layers in addition to measure the wear depth. However, an inaccuracy of 0.4 to 1.7 nm for the

graphene thickness has been reported the AFM [93]. Raman spectroscopy can be also used to determine the number of graphene layers. The difference between the two subpeaks is referred to as the splitting value of D' peak. The splitting of D' peak as a function of the number of graphene layers can be calculated through a fitting process involving the Lorentzian peaks [94]. The D' peak of a monolayer graphene is a single peak, while the D' peak of a few-layer graphene consists of subpeaks as shown in Figure 5 [95].

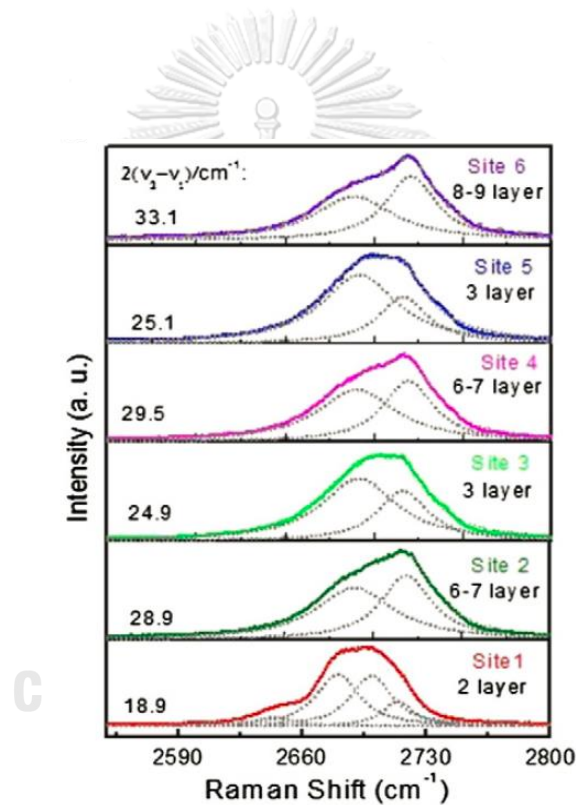


Figure 5 Raman spectra showing the D' peaks of different layers of graphene [95].

#### 2.6.4 Bonding (Adhesion) of Graphene to Metal

Surface adhesion properties are important parameter for studying the graphene/metal interaction for various applications [96]. Graphene interacts with the



surface of pure metals, carbides of various types metals, and alloys including Ni, Ti, and NiTi alloy with a strong reactivity with carbon [97]. Graphene interacts with each metals differently, and the graphene/metal interaction can be studied from the binding energy and interface separation.

Basically, two types of interactions have been found between graphene and metal substrate; chemisorbed (covalent) and physisorbed (noncovalent) [97-100]. In chemisorbed graphene, a relatively strong Pauli repulsion between graphene and the metal substrate is seen through a donation of electrons bonding, which is covalent in nature. Although the electronic interactions with the substrate significantly affect the electronic structure of graphene, the adsorption energy is still dominated by van der Waals interactions [98]. Whereas in physisorbed graphene, a weak Pauli repulsion equilibrates the van der Waals attraction;  $\pi$ - $\pi$  interactions, ionic interactions, and hydrogen bonding occur without affecting the electronic structure of the graphene. In addition, the D band electrons are mainly responsible for the bonding between graphene and metal [101]. A strong metal interaction occurs when their D band center lies between the Fermi level (highest energy state of electrons) and a binding energy of 2 eV, and weak interaction occurs with their binding energies of below 2 eV [97].

The binding energy of graphene/Ni is  $-1.29$  eV for Ni with an interface separation of  $2.1 \text{ \AA}$ , whereas that of graphene/Cu is  $-2.67$  eV, with an interface separation of  $3.3 \text{ \AA}$  [102]. The separation distance at a graphene/metal interface is directly related to its

electronic structure [97]. Graphene with a large separation from the substrate should show little change in its electronic structure, whereas a very strong interaction occurs when the energy of the lower frequency P band (250 to 500 MHz) is significantly altered [92]. Various factors affect the surface adhesion force of graphene on a metal substrate, such as the types of bond/interaction presented, the adhesion energy of multilayer graphene, the lattice structure, the hydrophobicity, and the roughness of the metal substrate. Abbas *et al.* [103] studied on the adhesion of graphene on Cu alloy using a tape test, and they found that hydrophobic surfaces ensure a good adhesion property. However, in our study, the hydrophobicity was not observed.

#### 2.6.5 Low Friction of Graphene

Graphene based coatings have been used in lubrication and reducing friction. The tribological properties of GO was studied by adding GO monolayer sheets to water-based lubricants that were applied to a sintered tungsten carbide ball and stainless steel flat plate [104]. Adding GO particles to water improved lubrication and provided a very low friction coefficient of approximately 0.05. Similar results were found by Berman *et al.* [105] who used graphene coating, and Lin *et al.* [95] who used a graphene platelet coating to reduce friction. Thus, graphene might be useful to reduce the friction of dental biomaterials such metal based prostheses used in dentistry [104].

## 2.7 Surface Modifications of NiTi Alloy

Researches have done to reduce the side effects of Ti and its alloys for better clinical applications with the surface modifications of NiTi and the development of new materials. The chief purpose of surface modification is to improve wear resistance, antibacterial property, bio-adhesion (bone ingrowth), and biocompatibility. Meanwhile, the important requirements such as adequate mechanical strength and processability are governed by the bulk material properties. Different surface modifications of NiTi alloy are done to enhance surface finishing (blasting, electro polishing), surface passivation (oxidation, nitriding), and surface coating [106].

## 2.8 Polymeric Coatings on NiTi Alloy

Polymer composite coatings over NiTi alloy has become a new approach to prevent the corrosion but the challenge is to preserve the bulk properties of the alloy. Successful coating includes biocompatible, very thin, good adhesion, good flexibility, hardness and strength. Both synthetic and natural polymers are being extensively studied as polymeric biomaterials. Various polymers and polymer composites that have been tried to coat NiTi alloys includes pyrrole [107], polypyrrole/HA nanocomposite [108], polyurethane (PU) [109], graphite–polyurethane [110], polyamide [69], polyetheretherketone [111], polytetrafluoroethylene [112], parylene [113], hexamethyldisilazane [114], and copolymer of N-isopropylacrylamide/ N-tert-

butylacrylamide [115]. The results of various polymer coatings tried for medical and dental applications from different techniques are shown in Table 4. Within the limitations of each research the polymer to some extent helps to improve the surface properties.

Table 4 Different polymer coatings on NiTi alloys for biomedical applications.

Polymer	Technique	Thickness	Results	Authors
HFMA	Plasma polymerization	NA	Coating increased in vitro hemocompatibility of NiTi for cardiovascular applications. Albumin/fibrinogen ratio increased and adherent platelets was reduced.	Li <i>et al.</i> 2014 [116]
PET and PU	NA	0.41 mm (Polyethylene) 0.02 mm (Polyurethane)	PET coated stents showed good biocompatibility. Mechanical properties were similar to NiTi stents. Polyurethane-coated stents showed often dislocation.	Schellhammer <i>et al.</i> 1999 [44]
PTFE	Plasma PVD Sputtering	50 nm and 100 nm	Nanocomposite PTFE coating on NiTi alloy was clear, thin, hydrophobic, stable with low friction coefficients (0.1 to 0.2).	Anjum <i>et al.</i> 2012 [112]

Polyamide	Dip coating	NA	Friction was lower. Ni release decreased by 85% in coated NiTi wires	Bravo <i>et al.</i> 2014 [69]
Parylene	Plasma polymerization	20 $\mu\text{m}$	Coated NiTi archwire had roughness 12 times lower.	Cho <i>et al.</i> 2013 [113]
PEEK and PEEK/Bioglass	EPD	3-5 $\mu\text{m}$	Coating on NiTi wire was uniform, homogeneous. PEEK and PEEK/Bioglass may be used for biomedical applications.	Boccaccini <i>et al.</i> 2006 [111]

HFMA: Hexafluorobutyl methacrylate; PET: Polyethylene terephthalate; PTFE: Polytetrafluoroethylene; PVD: Physical vapour deposition; HA: hydroxyapatite; PEEK: Polyetheretherketone.

Although various polymer composite coating has been tried on NiTi alloy, but there has always difficult to make successful coatings [44, 69, 107]. The drawbacks of polymers coating include porosity with release of toxic components and roughness [117]. With use, the polymer film may detach from the substrate or wire. Figure 6 shows the detachment of the pyrrole coating from NiTi alloy [107]. Research are focusing on development of biocompatible new composite coating with better and long-lasting performance.

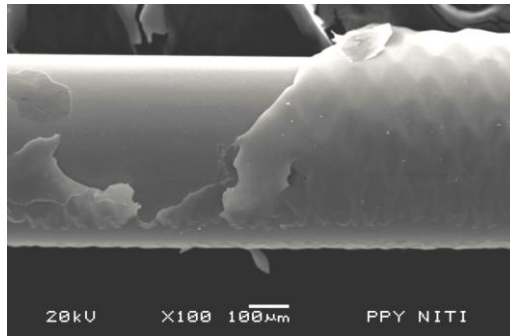


Figure 6 Detachment of a polymer (pyrrole) coating from NiTi alloy [107].

## 2.9 Graphene Coatings

Graphene based coatings have been well reported varying the performance [80, 118, 119]. The tribological behavior of GO layers at macro-scale is found to be not much different from that of the graphene layers [77]. The results confirm that GO may also be used to lubricate steel at macroscale by providing the coefficient of friction below 0.2. However, the wear rate stays at higher level than the ones for unmodified graphene. Berman *et al.* [105] found small amounts of graphene-containing ethanol solution decreased wear by almost 4 times and friction coefficients by a factor of 6 in sliding steel surfaces. Graphitic layers (which help in reducing friction and wear in artificial joints) have also been detected in metal-on-metal hip replacements [120]. The details of different studies of graphene and GO coatings on various substrates is shown in Table 5. The results from different studies show that the graphene coatings help to improve surface properties.

Table 5 Different studies of graphene and GO coatings on various substrates.

Coating	Method	Thickness	Results	Authors
Graphene	CVD technique at 450 °C	Few layers (20 μm)	Strong oxidation resistance was obtained on Cu substrate confirmed by SEM, Raman spectroscopy and XPS.	Kalita <i>et al.</i> 2014 [79]
Graphene	Mechanical Exfoliation	Multi-layer films (6-15 layers)	Graphene films exhibited much lower friction (0.36 to 0.62 nN) than bare Si surface (1.1 to 4.3 nN). Detectable wear of graphene was seen under 5 μN load from AFM.	Lin <i>et al.</i> 2011 [121]
GO	EPD	Multilayer	Friction reduced to 1/6 and wear reduced to 1/24 of its value.	Liang <i>et al.</i> 2013 [122]
Graphene	Direct application	Few-layers (2-3 layers)	Graphene-containing ethanol solution reduced wear by 4 times and friction by 6 times.	Berman <i>et al.</i> 2012 [105]

CHULALONGKORN UNIVERSITY

## 2.10 Silver Coatings

Silver or silver composite coatings can be developed from various methods, such as using chemical bath (electroless deposition) or EPD on various substrate for various applications [123-125]. The results of different studies of Ag-coatings on various substrates is shown in Table 6.

Table 6 Different studies of Ag-coatings on various substrates.

Coating	Method	Thickness	Results	Authors
Ag film	Chemical bath	NA	Thin Ag films on glass (SiO <sub>2</sub> ) were investigated by SEM and Raman spectroscopy. Fine-grained films exhibited 3 structures; fine nuclei on the glass, isolated strands of small crystals and individual octahedral micron-sized single crystals on surface.	Buckley and Hope. 2006 [123]
Ag film	Chemical bath	NA	Conductivity of the Ag films was determined by Raman spectroscopy.	Naor and Avnir. [124]
Ag and Ag/Cu/ruthenium (Ru)	EPD	Multilayer	Ag and Ag/Cu/Ru multilayer prepared on Ru substrate were by electrodeposition.	Cheng <i>et al.</i> 2003. [125]
Ag film	Chemical bath	Multilayer	Ultrafine Ag particles were anchored on Tin (Sn)-Ag membrane.	Byeon and Kim. [126]

## 2.11 Graphene Nanocomposite Coatings

Various GO nanocomposites are fabricated to improve the properties (friction coefficient) of the coating [81, 127]. GO/Ag nanocomposites helped to inhibit microbial growth (*P. aeruginosa*) and prevent biofilm formation [90]. The nanocomposites could



be effective for the treatment of both cancer [128]. The details of different studies of graphene nanocomposite coatings on various substrates is shown in Table 7.

Table 7 Different studies of graphene nanocomposite coatings on various substrates.

Coating	Method	Thickness	Results	Authors
Ag nanopartic les doped GO	In situ polymeriza tion in solution	NA	Pseudo capacitive properties increased in the Ag doped samples resulting in an increase of the capacitance. It could be a good conductive electrode for energy storage devices and electrochemical sensors.	Tran <i>et al.</i> 2015 [129]
GO sheets decorated with Ag nanopartic les (GO– Ag).	Solution processed using Na (citrate as stabilizing agent)	NA	GO–Ag nanocomposites inhibited growth of microbial ( <i>P. aeruginosa</i> ) adhered cells and preventing biofilm formation on stainless steel.	de Faria <i>et al.</i> 2014. [90]
rGO–Ag nanopartic le nanocomp osites	Analytical techniques. <i>Tilia amurensis</i> plant extracts: (TAPE)	NA	rGO–Ag nanocomposites could be used for the treatment of cancer.	Gurunath an <i>et al.</i> 2015 [128]

## 2.12 Conceptual Framework of this Research

Figure 7 shows the conceptual framework of our research. The factors that might affect the coatings includes alloy factor, solution factor and coating process.

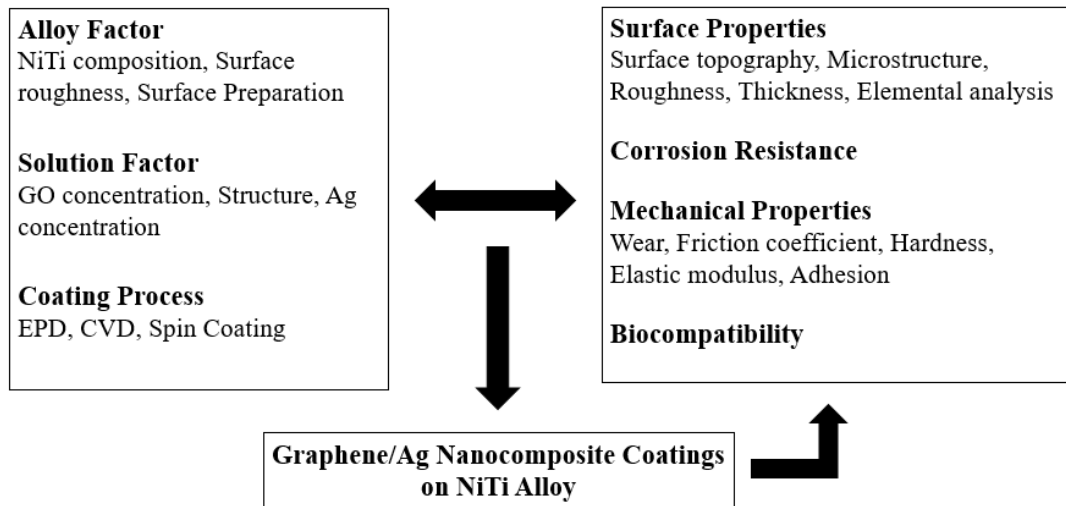


Figure 7 Conceptual framework of the study.

Hence, our study aims to develop a GO and GO/Ag nanocomposite coating on NiTi alloy and study the surface properties (surface structure, topography, roughness and thickness), mechanical properties (friction and wear, hardness, modulus of elasticity, and surface adhesion), and biocompatibility of the GO and GO/Ag nanocomposite coated NiTi alloy.

## CHAPTER III

### MATERIALS AND METHODS

#### 3.1 Overview of this Study

The overview of the experiment details of this study is shown in Figure 8.

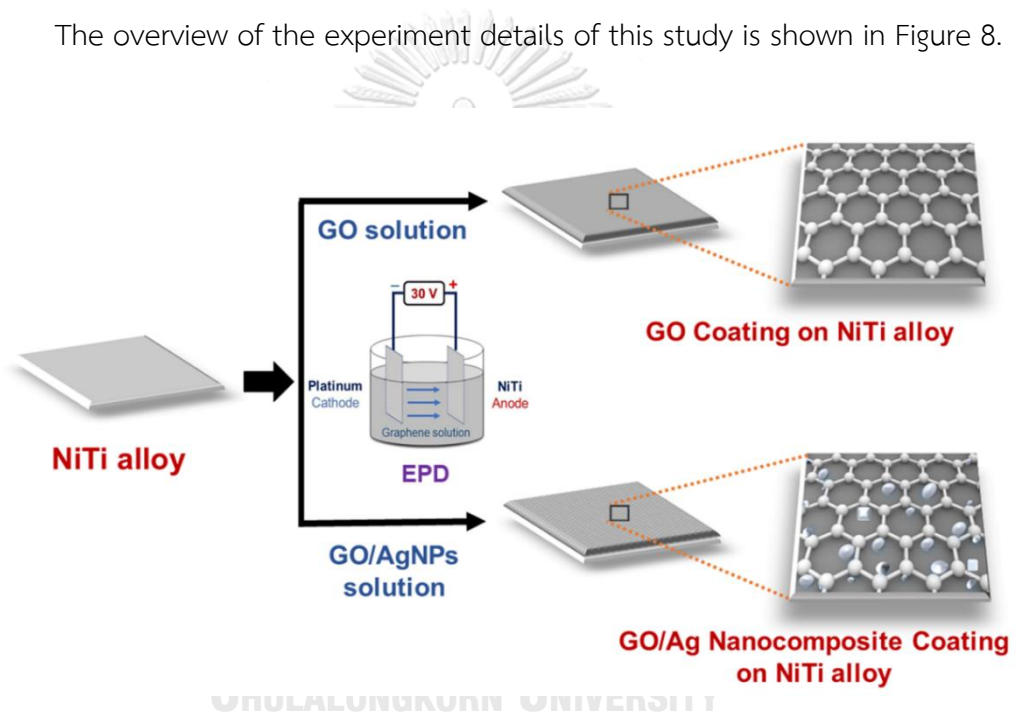


Figure 8 Overview of the experiment details this study.

#### 3.2 Sample Preparation

Medical grade NiTi alloy substrates consisting of Ni (55.7 wt%), Ti (44.8 wt%), and other elements (0.2 wt%) (Baoji Seabird Metal Material Co., Ltd, China) were cut into 40 x 20 x 1 mm plates. The NiTi alloy substrates were polished with silicon carbide

paper up to 2000 grit to remove oxide layer and to obtain a uniform roughness for the adhesion of the coating. The NiTi alloy substrates were ultrasonically cleaned by sequential immersion in acetone, ethanol, and DI water for 10 min each. The substrates were placed in Kroll's reagent consisting of 2 ml 40% nitric acid, 4 ml 40% hydrofluoric acid, and 994 ml DI water for 10 min to remove any remaining oxide layer. Finally, the substrates were dried after rinsing in DI water.

### 3.3 Graphene Oxide (GO) Solution Preparation

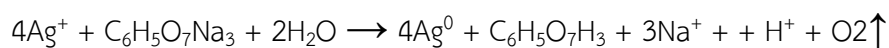
GO powder with average diameter 50  $\mu\text{m}$  (Nanjing Jing Ji Cang Nano Technology Co., Nanjing, China) produced by a modified Hummers' method was used in this study [11]. The GO was produced by a graphite oxidation process using potassium permanganate ( $\text{KMnO}_4$ ) and concentrated sulfuric acid ( $\text{H}_2\text{SO}_4$ ). A 100 ml GO solution (0.01 mg/ml) was prepared in deionized (DI) water and ultrasonicated for 3 h.



### 3.4 GO/AgNPs Solution Preparation

A 100 ml silver nitrate ( $\text{AgNO}_3$ ) (Pure P.A., Gliwice, Poland) solution (0.1 mg/ml) was prepared and ultrasonicated for 20 min. The GO and  $\text{AgNO}_3$  solutions were mixed and ultrasonicated for 30 min. Finally, a AgNPs solution was produced by chemical reduction using trisodium citrate ( $\text{Na}_3\text{C}_6\text{H}_5\text{O}_7$ ) (tri-Sodium Citrate dihydrate, Carlo Erba Reagents, Val-de-Reuil, France) as a stabilizing agent [130]. The GO/ $\text{AgNO}_3$  solution

was heated at 80°C for 1 h and 10 ml of Na<sub>3</sub>C<sub>6</sub>H<sub>5</sub>O<sub>7</sub> (0.01 mg/ml) was added dropwise. The solution was maintained at 80°C for 1 h and ultrasonicated for 20 min at room temperature to obtain a homogeneous GO/AgNPs mixture. The mechanism of reaction is expressed as follows:



### 3.5 EPD of GO and GO/AgNPs

The potential of the suspension of GO and GO/Ag were measured by using a zeta potentiometer. A negative potential was found, i.e. -38 mV for GO and -39 mV was obtained. Hence, the NiTi alloy substrates served as the anode (+) and the platinum metal served as the cathode (-). Two solutions were made; graphene solution and GO/AgNPs solution. The two electrodes were immersed in each solution parallel to each other 15 mm apart. Three EDP coating duration groups were prepared from. EPD was performed for 1 min, 5 min, or 10 min with slow magnetic stirrer at a constant voltage of 30 V. After EDP, the graphene and GO/Ag nanocomposite coated substrates were removed from the solution and rinsed with DI water, and dried at room temperature for 24 h and kept at 80°C for 5 h.

The samples were names as GO1, GO5, GO10 for GO-coated NiTi alloys and GOAg1, GOAg5, GOAg10 for GO/Ag-coated groups for each 1min, 5min, and 10 min,

respectively. After the coating process, three properties were tested; surface characteristics, mechanical properties, and biocompatibility.

### 3.6 Surface Characterization of the Coatings

The surface morphology of the GO and the GO/Ag coated NiTi alloys substrates was observed using scanning electron microscopy (SEM) (Quanta 250, FEI Co., Helsinki, Finland) with an operating voltage of 30 kV and surface profilometer (Taylor Scan 150, Taylor Hobson Ltd., Leicester, UK). Elemental analysis of the coatings was performed using energy dispersive spectroscopy (EDS). Raman spectra were studied from Raman spectroscopy (LamRAM HR, Horiba Scientific Inc., New York, USA) equipped with solid-state laser with the diode pumped at 532 nm with a grating of 1200 gr/mm and a 200  $\mu\text{m}$  slit.

### 3.7 Mechanical Properties of the Coatings

The following mechanical properties of the GO and the GO/Ag Nanocomposite coating on NiTi studied were:

- Coating Thickness and Roughness
- Friction Coefficient
- Hardness and Modulus of Elasticity
- Surface Adhesion Force and Energy

### 3.7.1 Coating Thickness and Surface Roughness

The coatings thickness and surface roughness (Ra) of the GO and GO/Ag coatings were evaluated from the surface profilometer. The surface roughness of the coatings was measured from the surfaces of the bare and coated substrates, whereas the thickness of the coatings was measured from the coated substrates from the step height profile. The mean Ra and thickness of the coatings were measured from ten times for each sample.

### 3.7.3 Friction Coefficient

The friction coefficient of the GO coating and the GO/Ag nanocomposite coatings on NiTi alloy were tested using a ball-on-disc micro-tribometer by sliding them against a steel ball of 6 mm in diameter in a circular path of 5 mm in radius for 1.90 m at sliding speed of 60 rpm (0.0314 m/s) for 60 seconds under a normal constant load of 0.2 N at 27°C temperature and 60% relative humidity.

### 3.7.4 Hardness and Modulus of Elasticity

The hardness and modulus of elasticity the GO coating and GO/Ag nanocomposite coating on NiTi alloy were measured using a nano-indenter (Nanoindenter II, NanoInstruments, CSIRO, Australia) with a Berkovich (pyramidal shape)

diamond tip as described by Poon et al. [131]. Six measurements were measured for each sample. The diamond stylus used in the unit is in the form of a cone with a spherical tip of 0.2 mm in radius at a 3 mN load for 1.14 min per indentation. The mean hardness and modulus of elasticity of the coatings were calculated from 6 indentations made on each sample.

### 3.7.5 Adhesion Force and Energy

An atomic force microscope (AFM) (NX10, Park System, Suwan, South Korea) in contact mode was used to study the surface structure, surface adhesion force (maximum unbinding force), and surface adhesion energy of the GO and GO/Ag coating using a CONTSCR nano tip of 105  $\mu\text{m}$  in length and 15  $\mu\text{m}$  in height, with a sensitivity of 43.056  $\text{V}/\mu\text{m}$  at a frequency of 23 KHz, and a constant force of 0.2 N/m at 27 °C with 60% relative humidity. The measurements were done 20 times, and the mean was calculated.



### 3.8 Biocompatibility of the Coatings

The biocompatibility of the GO and the GO/Ag coatings on NiTi alloys were determined using a 3-[4,5-dimethylthiazol-2-yl]-2, 5-diphenyltetrazolium bromide (MTT) assay following the approval of the study protocol by The Human Research



Ethics Committee of the Faculty of Dentistry, Chulalongkorn University (Protocol No. HREC-DCU 2018-084).

### 3.8.1 Cell Culture

Human gingival fibroblasts were explanted from gingiva of patients. The inclusion criteria of the participants include healthy patients with sound soft tissues around the third molar to be extracted, caries (if present) limited to pulp without periapical lesions. Exclusion criteria includes systemic disease, infection around the third molar and pregnant women.

Human gingival fibroblasts were obtained from the extracted third molars as described by Jettanacheawchankit *et al.* [132]. The gingiva was minced and the pieces were placed on 35-mm culture plates. The cells were cultured in growth media [Dulbeccous Modified Eagle Medium (DMEM) supplemented with 100 IU/ml penicillin, 100  $\mu$ g/ml streptomycin, 25  $\mu$ g/ml amphotericin, 2 mM L-glutamine, and 10% fetal bovine serum]. The medium was changed every two days. The cells were cultured at 37°C in a humidified 5% CO<sub>2</sub> atmosphere. When the cells reached 80% confluence, the cells were sub-cultured using 0.25% trypsin-EDTA. All cell culture media were purchased from GibcoBRLTM (InvitrogenTM, Grand Island, NY, USA).

### 3.8.2 MTT Cytotoxicity Assay

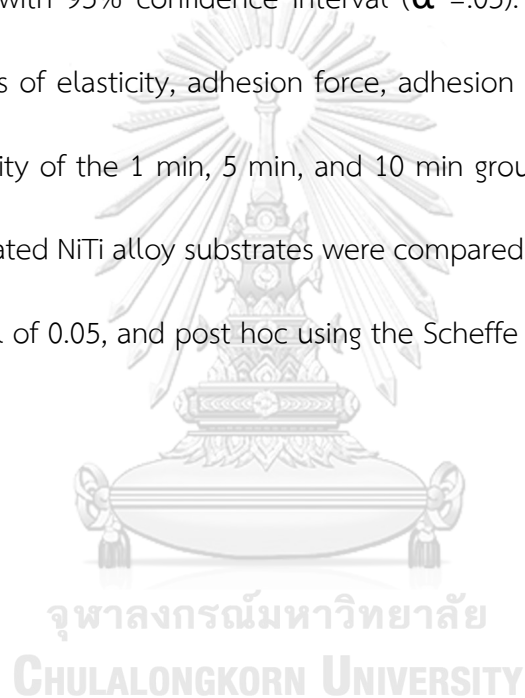
GO-coated and GO/Ag-coated NiTi specimens were reduced to 3 × 6 mm and autoclaved. Each specimen was immersed in 5 ml of growth media at 37°C for 24 h. For the control group, the same volume of growth media was incubated under the same conditions.

The MTT test was conducted as previously described with some modifications (Zhang et al., 2013). Briefly, 50,000 cells/well were seeded into a 48 well culture plate (Nunc™ cell culture plate, Thermo Scientific, USA). After 24 h, the cells were washed with phosphate buffered saline twice (PBS) and then incubated with the conditioned medium (250 µL) of each the GO-coated, the GO/Ag-coated NiTi specimens, and growth medium (control group) for 24 h. After 24 h, the cells were again washed twice with PBS and incubated with 0.5 mg/mL of MTT solution prepared from MTT reagent (*Invitrogen, Molecular Probes, Oregon, USA*) for 10 min. The precipitated formazan crystals were dissolved in dimethyl sulfoxide (DMSO) and the optical densities of the solutions were measured at an absorbance of 570 nm. The assays were performed in 3 independent experiments. The number of viable cells after exposure to the conditioned medium of GO-coated and GO/Ag-coated NiTi alloys were calculated from the straight-line equation ( $y = mx + c$ , where  $m$  is the **slope** of the line, and  $c$  is the **y intercept**) and compared with the control. The cells were examined with an Olympus

light microscope (Olympus, U-CMAD3, Tokyo, Japan) at 4x, 10x, and 20x magnifications and images were taken.

### 3.9 Statistical Analysis

All data were analyzed using SPSS 18 statistical software for Windows (SPSS, Chicago, IL, USA) with 95% confidence interval ( $\alpha = .05$ ). The thickness, roughness, hardness, modulus of elasticity, adhesion force, adhesion energy, friction coefficient, and biocompatibility of the 1 min, 5 min, and 10 min groups of both the GO-coated and the GO/Ag-coated NiTi alloy substrates were compared using a one-way ANOVA at a significance level of 0.05, and post hoc using the Scheffe test.



## CHAPTER IV

### RESULTS

We successfully prepared GO and GO/Ag coatings on NiTi alloy using EPD, and studied the surface properties, mechanical properties, and biocompatibility as shown below.

#### 4.1 Results of Surface Characterization of NiTi alloy

The surface morphology of bare NiTi substrate determined from SEM/ EDS, surface profilometer and AFM is shown in Figure 9. The images show that the surface morphology of the NiTi substrates was rough with some voids.

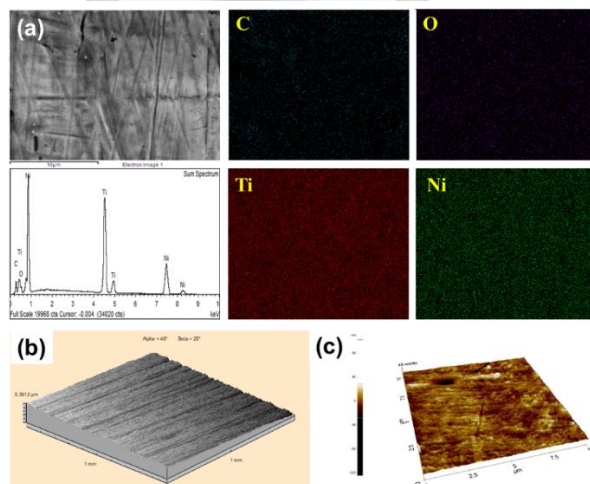


Figure 9 Surface morphology of the bare NiTi substrates obtained from: (a) SEM/EDS and (b) surface profilometer and (c) AFM.

## 4.2 Results of Surface Characterization of the Coatings

The results of surface characterizations of the coatings are shown below.

### 4.2.1 SEM/ EDS

Figure 10 and Figure 11 shows SEM images and EDS mapping of GO-coated and GO/Ag-coated NiTi alloys, respectively. The surface morphology of the coated alloys was homogeneous with some voids with no cracks.

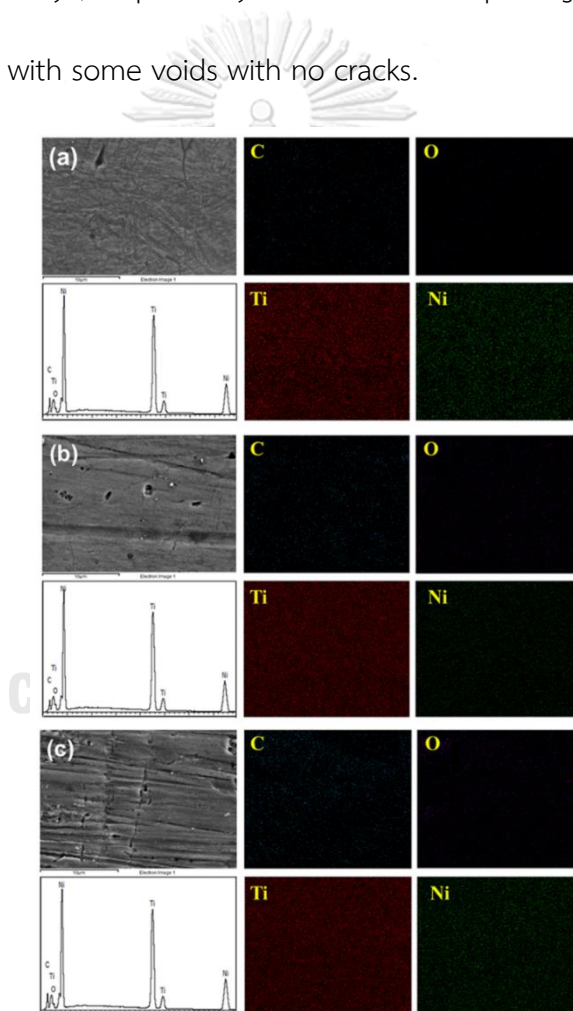


Figure 10 SEM/ EDS images of the GO-coated NiTi alloy: (a) 1 min, (b) 5 min, and (c) 10 min.

The surface morphologies of the GO-coated alloys are similar to the GO/Ag-coated NiTi alloys but EDS analysis shows the presence of Ag in the GO/Ag coatings (Figure 10 and Figure 11).

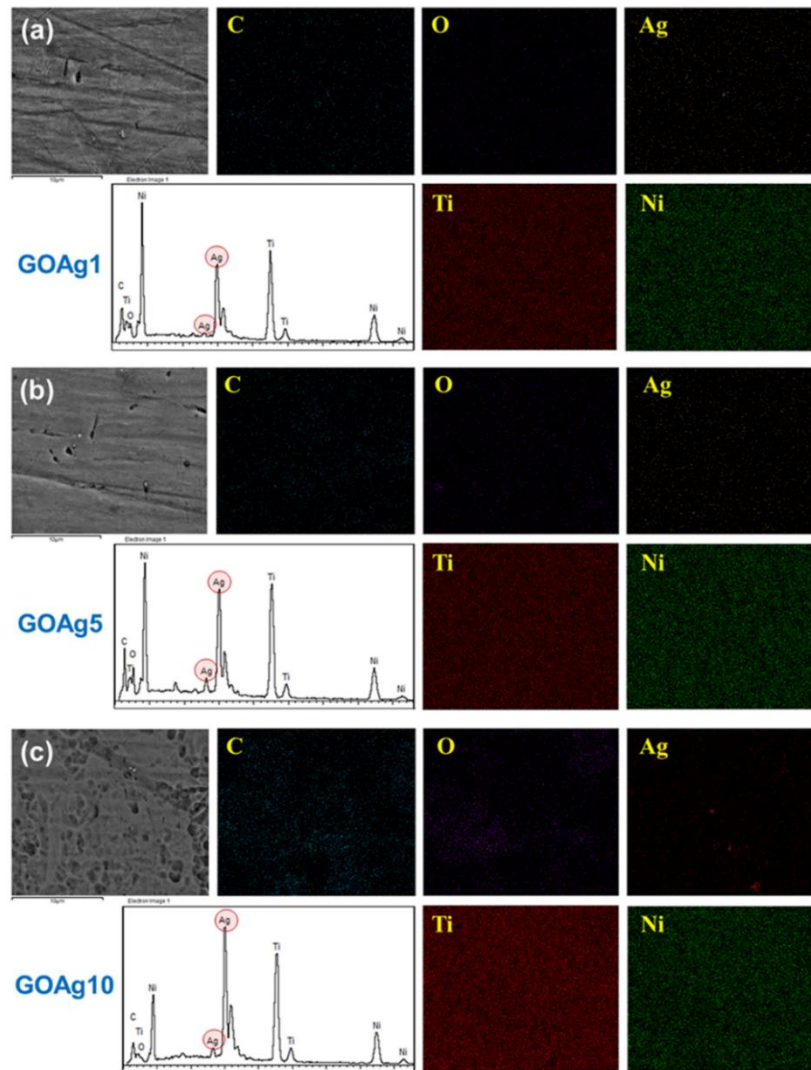


Figure 11 SEM/EDS images of the GO/Ag-coated NiTi alloy: (a) 1 min, (b) 5 min, and (c) 10 min. Ag ions are marked in each EDS spectrum. Ag ions are marked in the EDS spectrum.

The EDS elemental analysis of the GO-coated and the GO/Ag-coated NiTi alloys are shown in Figure 12. The EDS elemental analysis showed that the Ni and Ti concentration decreased with coating time, and the C and O concentration increased with coating time in both GO-coated and GO/Ag-coated NiTi alloys compared to bare NiTi alloy. In addition, the concentration of AgNPs in the GO/Ag coatings increased with increased coating time.

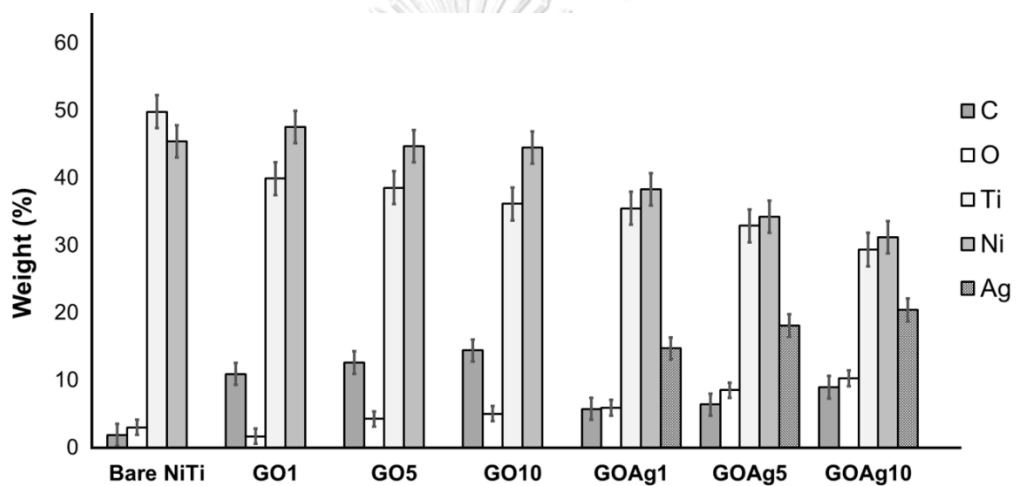


Figure 12 EDS elemental analysis (wt%) of the GO-coated and the GO/Ag-coated NiTi alloy substrates.

#### 4.2.2 Surface Profilometry

The surface morphology of the bare NiTi substrates from surface profilometry shows rough with some surface voids. They show similar surface morphology similar to SEM. The optical surface images from surface profilometer of the bare NiTi alloy and the coated (GO-coated and GO/Ag-coated) substrates are shown in Figure 13. The

surface morphology of the coated NiTi alloys were homogeneous with some voids and no cracks.

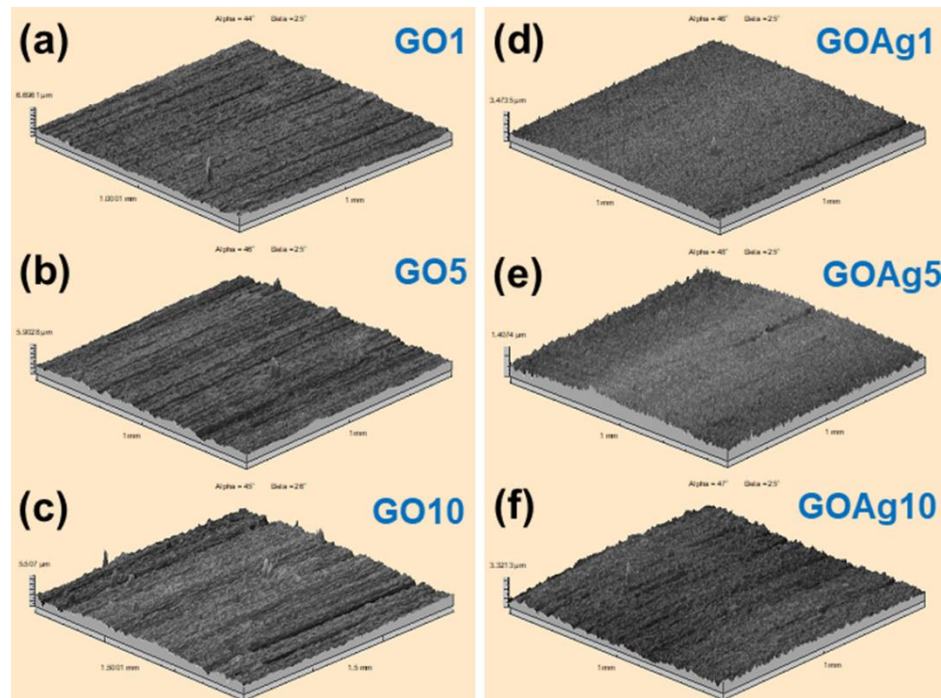


Figure 13 Surface profilometer images of the GO-coated (a, b, c) and the GO/Ag-coated (d, e, f) NiTi alloy substrates for 1 min (a, d), 5 min (b, e), and 10 min (c, f).

#### 4.2.3 Raman Spectroscopy

In this study, the Raman spectra of the both GO-coated and GO/Ag-coated NiTi substrates show D and G bands (Figure 14). For GO coating, the D bands ranged from 1342 to 1346  $\text{cm}^{-1}$  and G bands ranged from 1590 to 1603  $\text{cm}^{-1}$ . Similarly, for the GO/Ag nanocomposite coating, D bands ranged from 1340 to 1344  $\text{cm}^{-1}$  and G bands ranged from 1599 to 1604  $\text{cm}^{-1}$ . In addition, the  $I_D/I_G$  ratio was 0.84 for both GO-coated and GO/Ag-coated NiTi substrates.



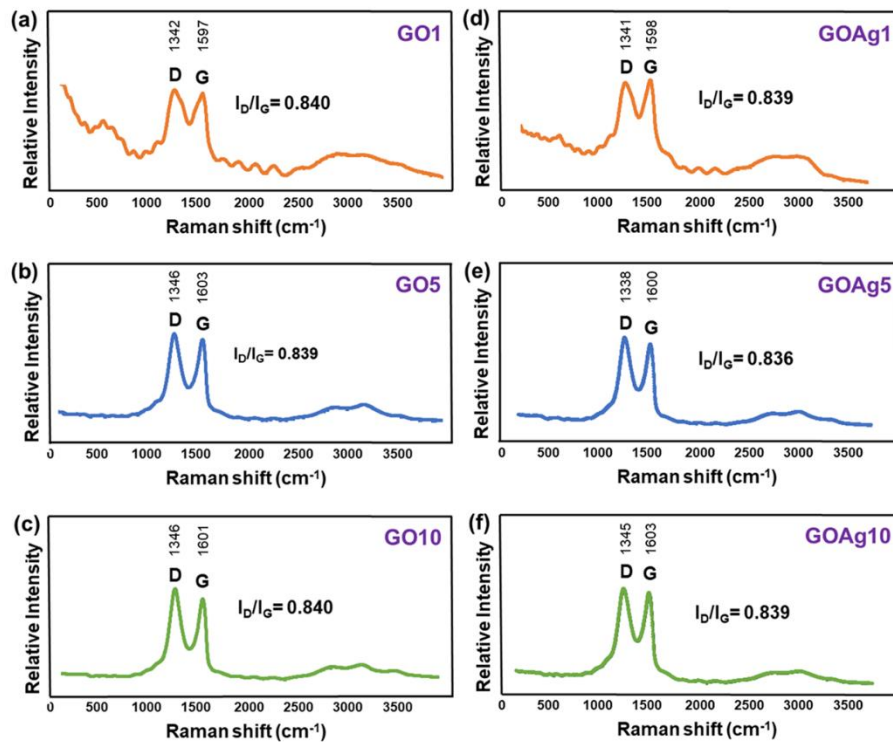


Figure 14 Raman spectra of the GO-coated NiTi alloys of coating time: (a) 1 min, (b) 5 min, and (c) 10 min groups, and the GO/Ag-coated NiTi alloys of coating time: (d) 1 min, (e) 5 min, and (f) 10 min groups.

#### 4.2.4 Atomic Fluorescopy Microscopy (AFM)

AFM images and points for the measurement of the adhesion force and energy of the GO-coated and the GO/Ag-coated NiTi alloys are shown in Figure 15 and Figure 16, respectively. The contact-mode AFM was used to measure the adhesion force and energy of the GO-coated and the GO/Ag-coated NiTi alloys using the CONTSCR nano tip.

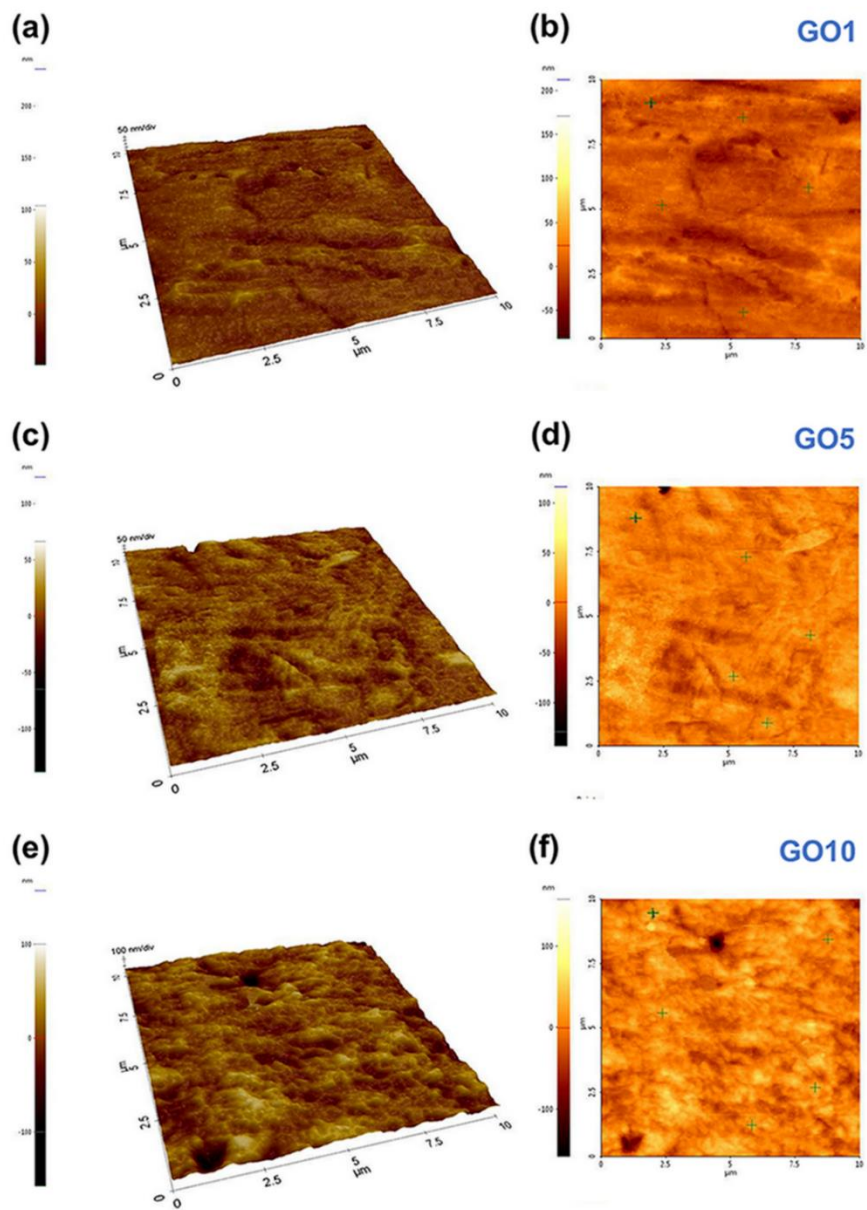


Figure 15 AFM images and points for the measurement of adhesion force and energy using the contact-mode AFM with CONTSCR nano tip on the GO-coated NiTi alloy substrates for 1 min: (a) and (b), 5 min: (c) and (d), and 10 min: (e) and (f), respectively.

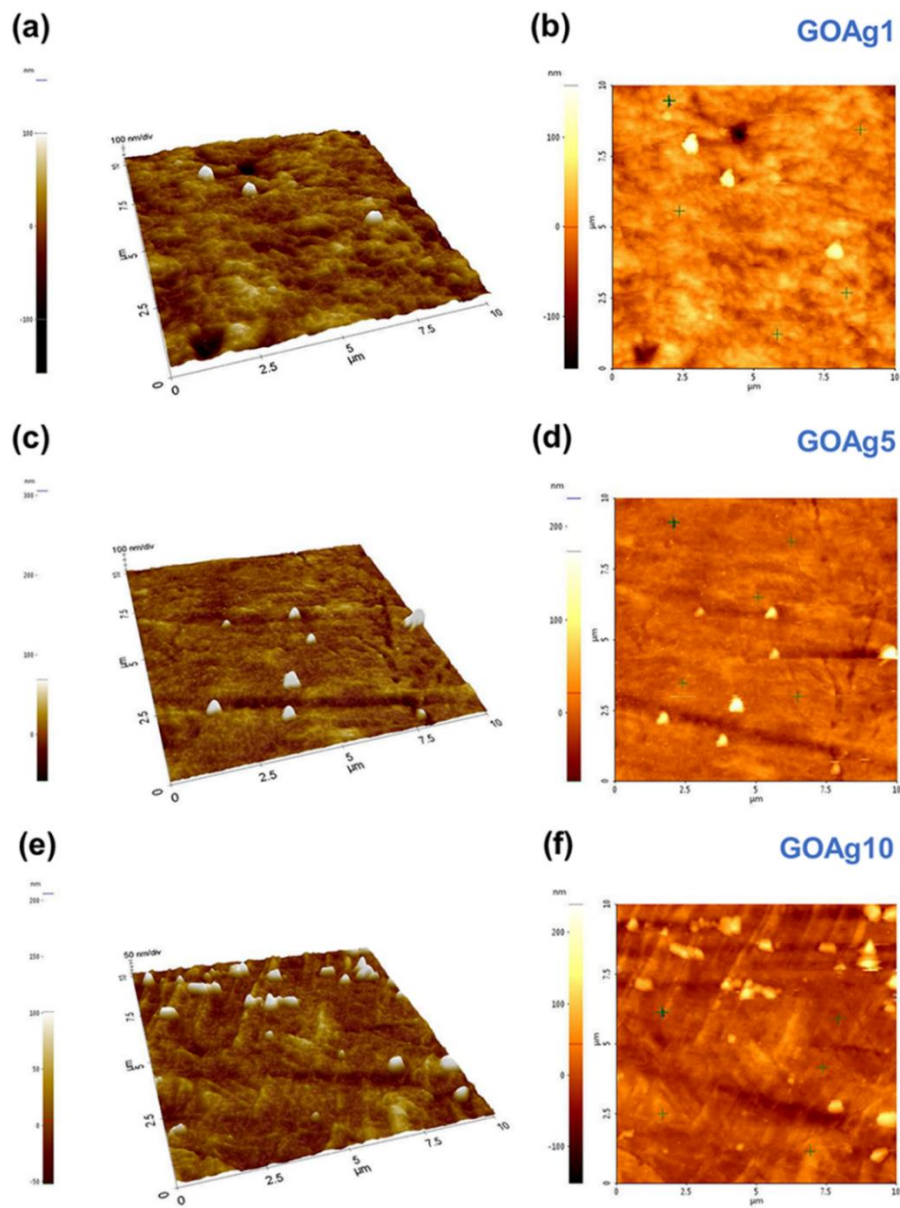


Figure 16 AFM images and points for the measurement of adhesion force and energy using the contact-mode AFM with CONTSCR nano tip on the GO/Ag-coated NiTi alloy substrates for 1 min: (a) and (b), 5 min: (c) and (d), and 10 min: (e) and (f), respectively.

### 4.3 Results of Coatings Thickness and Surface Roughness

The results of the mean thickness of the GO and the GO/Ag coatings on a NiTi substrate are also shown in Figure 17. The thickness of the GO coatings ranged from 0.34 to 1.12  $\mu\text{m}$  and for the GO/Ag coatings ranged from 0.48 to 1.38  $\mu\text{m}$ . The mean thickness of GO1 was  $0.344 \pm 0.143 \mu\text{m}$ , GO5 was  $0.651 \pm 0.107 \mu\text{m}$ , and GO10 was  $1.327 \pm 0.095 \mu\text{m}$ . Similarly, the mean thickness of GOAg1 was  $0.482 \pm 0.063 \mu\text{m}$ , GOAg5 was  $0.763 \pm 0.281 \mu\text{m}$ , and GOAg10 was  $1.385 \pm 0.097 \mu\text{m}$ . For both GO and GO/Ag coatings, there was significant difference among 1 min, 5 min and 10 min coatings ( $< 0.05$ ). In addition, it showed that the thickness of both GO and GO/Ag coating increased with the increased coating time.

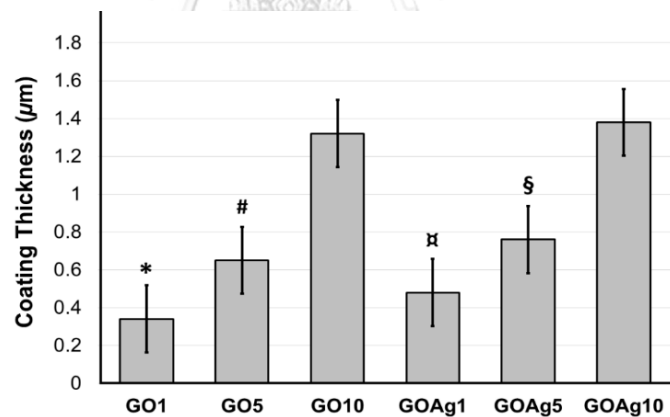


Figure 17 Coating thickness of the GO and the GO/Ag coatings on NiTi alloy substrates. \* denotes the significant different from GO5 ( $P = 0.005$ ) and GO10 ( $P < 0.001$ ). # denotes significant different from GO1 ( $P = 0.005$ ) and GO10 ( $P < 0.001$ ).  $\alpha$  denotes significant different from GO5 ( $P = 0.045$ ) and GOAg10 ( $P < 0.005$ ). § denotes significant different ( $P < 0.05$ ) from GOAg10 ( $P < 0.001$ ).

The surface roughness (Ra) of the GO-coated alloy ranged from 49.92 to 66.55 nm and the GO/Ag-coated alloy ranged from 52.28 to 68.03 nm (Figure 18). The coated substrates showed higher roughness than that of the bare NiTi alloys (31.85 nm). It showed that the surface roughness of both the GO-coated and the GO/Ag-coated NiTi alloy substrates was significantly higher compared to the bare NiTi alloy ( $P < 0.001$ ). Furthermore, the surface roughness of GO1 showed statistically significant different ( $P < 0.001$ ) from GO5 and GO10, and GO5 showed significant different ( $P < 0.001$ ) from the GO1. Similarly, the surface roughness of GOAg1 showed presented statistically significant different ( $P < 0.001$ ) from GOAg5 and GOAg10, and GOAg5 showed statistically significant different ( $P < 0.001$ ) from GOAg1. The surface roughness of both the GO and the GO/Ag coatings increased with coating time.

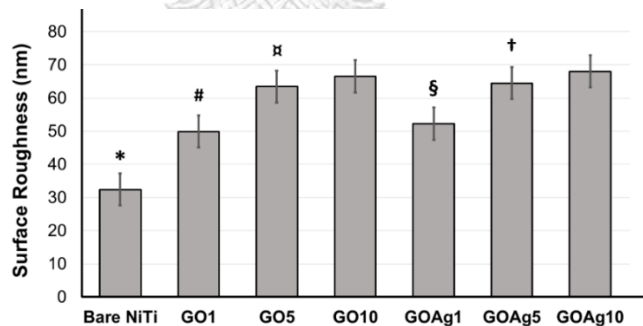


Figure 18 Surface roughness of the bare NiTi, the GO and the GO/Ag coatings on NiTi alloy substrates. \* denotes significant different ( $P < 0.001$ ) from GO-coated (GO1, GO5, GO10) and GO/Ag coated (GOAg1, GOAg5, GOAg10). # denotes significant different ( $P < 0.001$ ) from GO5, GO10 and bare NiTi. α denotes significant different ( $P < 0.001$ ) from GO1 and bare NiTi. § denotes significant different ( $P < 0.001$ ) from GOAg5, GOAg10 and bare NiTi. † denotes significant different ( $P < 0.001$ ) from GOAg1 and bare NiTi.

#### 4.4 Results of Surface Adhesion Properties

The results of the surface adhesion force and adhesion energy of the GO-coated and the GO/Ag-coated NiTi alloys are also shown in Figure 19. The surface adhesion force for the GO-coated NiTi alloy substrates ranged from 3.71 to 14.8 nN, and for the GO-coated NiTi alloys ranged from 3.35 to 15.33 nN. For both the GO-coated and the GO/Ag-coated NiTi alloy substrates, 1 min coatings showed the highest surface adhesion force, followed by 10 min and then 5 min. The results of the surface adhesion force of the GO-coated and the GO/Ag-coated NiTi alloy substrates showed a non-linear pattern of the surface adhesion force and energy of the GO-coated and GO/Ag-coated NiTi alloy substrates for different coating times.

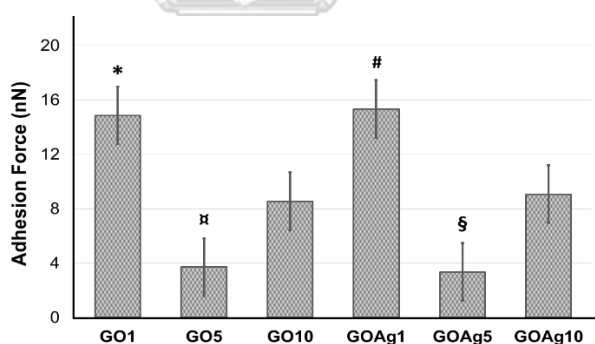


Figure 19 Surface adhesion force measured from AFM of the GO-coated and the GO/Ag-coated NiTi alloy substrates. \* denotes significant different ( $P < 0.05$ ) from GO5 and GO10. α denotes the significant different ( $P < 0.05$ ) from GO1 and GO10. # denotes significant different ( $P < 0.05$ ) from GOAg5 and GOAg10. § denotes the significant different ( $P < 0.05$ ) from GOAg1 and GOAg10.

Multiple comparison of surface adhesion showed the significant different ( $P < 0.05$ ) among all groups of GO-coated (GO1, GO5 and GO10) and GO/Ag-coated (GOAg1, GOAg5 and GOAg10) NiTi alloys.

The adhesion energy ranged from 0.23 to 0.69 mJ/m<sup>2</sup> for GO-coated NiTi alloys and from 0.24 to 0.71 mJ/m<sup>2</sup> for GO/Ag-coated NiTi alloys. The surface adhesion energy also followed a similar non-linear pattern as that of the adhesion force for both GO-coated and GO/Ag-coated NiTi alloy substrates (Figure 20). There was significant difference ( $P < 0.05$ ) among all the GO-coated groups but no significant difference ( $P = 0.09$ ) between GOAg1 and GOAg10 for the surface energy.

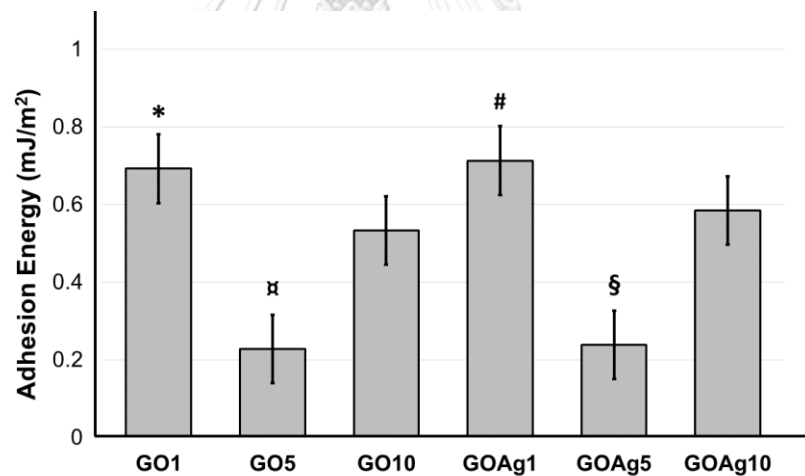


Figure 20 Surface adhesion energy measured from AFM of the GO-coated and the GO/Ag-coated NiTi alloy substrates. \* denotes significant different ( $P < 0.05$ ) from GO5 and GO10. α denotes the significant different ( $P < 0.05$ ) from GO1 and GO10. # denotes significant different ( $P < 0.05$ ) from GOAg5 and GOAg10. § denotes the significant different ( $P < 0.05$ ) from GOAg5 ( $P < 0.05$ ).

#### 4.5 Results of the Friction Coefficient

We determined the friction coefficient of the bare NiTi alloy and the coated substrates (Figure 21). The bare NiTi substrate demonstrated significantly higher friction coefficient ( $0.061 \pm 0.049$ ) compared to both GO-coated ( $0.022 \pm 0.014$  for GO1,  $0.013 \pm 0.11$  for GO5, and  $0.006 \pm 0.005$  for GO10), and GO/Ag-coated groups ( $0.023 \pm 0.021$  for GOAg1,  $0.015 \pm 0.013$  for GOAg5, and  $0.006 \pm 0.005$  for GOAg10). In addition, the friction coefficient of the GO-coated and GO/Ag-coated groups were significantly lower than the bare NiTi alloy ( $P < 0.001$ ). The friction coefficients of 1 min coated samples of both groups (GO1 and GOAg1) showed statistically significant different ( $P < 0.05$ ) from 10 min coated samples (GO10 and GOAg10).

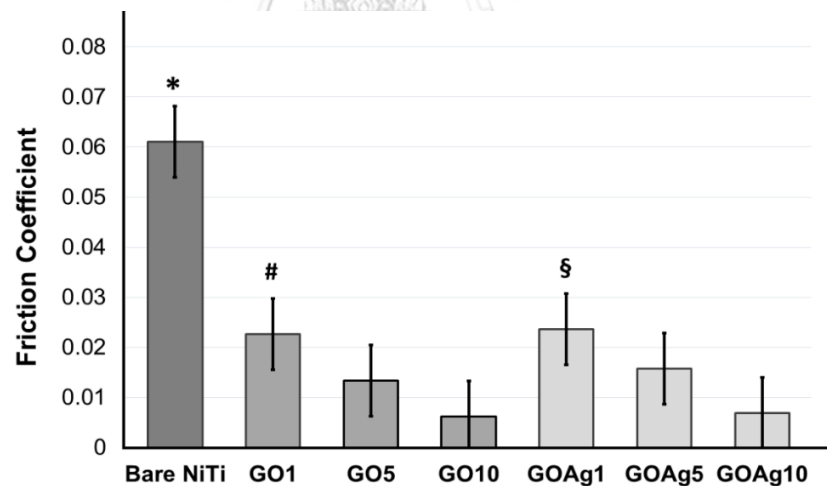


Figure 21 Friction coefficient of the bare, the GO-coated and the GO/Ag-coated NiTi alloy substrates. \* denotes significant different ( $P < 0.001$ ) from GO-coated (GO1, GO5, GO10) and GO/Ag coated (GOAg1, GOAg5, GOAg10). # denotes the significant difference ( $P > 0.05$ ) from GO10. § denotes the significant difference ( $P < 0.05$ ) from GOAg10.



#### 4.6 Results of the Hardness and Modulus of Elasticity the Coatings

The results of Berkovich hardness of the coated NiTi alloy substrates is shown in Figure 22. The hardness of the GO-coated NiTi alloys ranged from 0.41 to 0.88 GPa, and hardness of the GO/Ag-coated NiTi alloys ranged from 0.44 to 0.92 GPa. In both, the GO-coated and the GO/Ag-coated groups, the hardness decreased with increasing coating time from 1 min to 5 min and then became stable, and there was significant difference ( $P < 0.001$ ) between 1 vs 5 min, and 1 vs 10 min coatings.

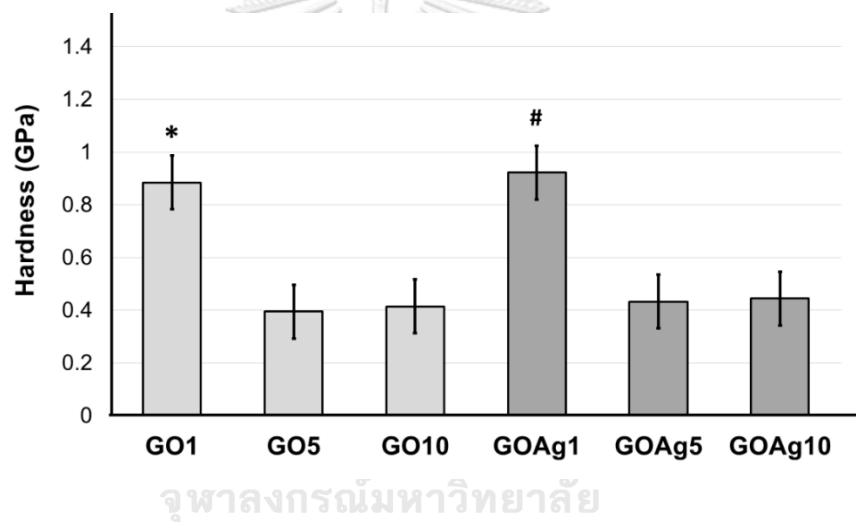


Figure 22 Berkovich hardness of the GO-coated and the GO/Ag-coated NiTi alloy substrates of coating time. \* denotes the significant difference ( $P < 0.001$ ) from GO5 and GO10. # denotes significant difference ( $P < 0.001$ ) from GOAg5 and GOAg10.

The results of modulus of elasticity the GO and GO/Ag coatings is shown in Figure 23. The modulus of elasticity the GO-coatings ranged from 1.13 to 4.25 GPa, and the GO/Ag-coatings ranged from 1.15 to 4.89 GPa. The modulus of elasticity of the GO-coated and the GO/Ag-coated groups increased with increased coating time from 1 to 10 min and there was significant difference ( $P < 0.001$ ) between 1 vs 5 min, and 1 vs 10

min coatings. Increasing coating time, increased the thickness of the graphene coatings which caused more interactions with the indenter. Hence, the graphene coating showed better elastic recovery and resisted more against the deformation caused from load application.

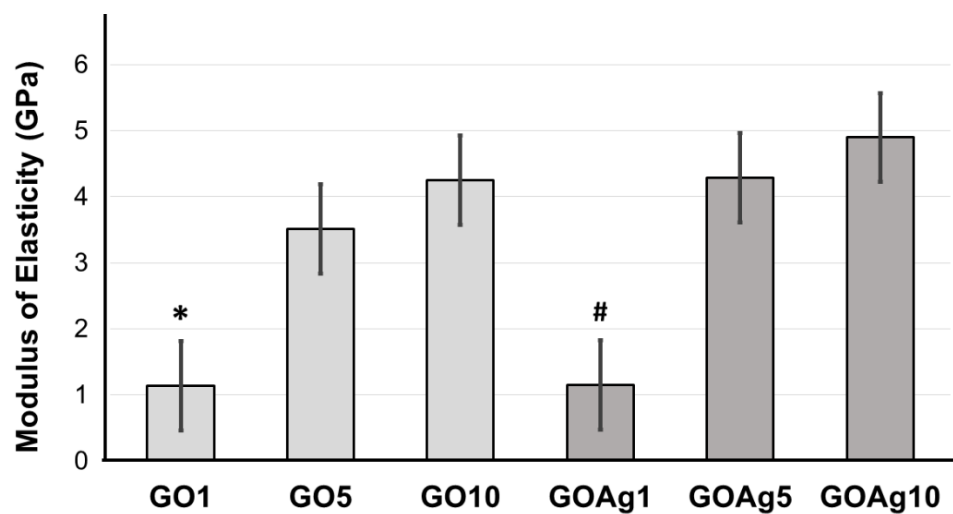


Figure 23 Modulus of elasticity of the GO-coated and the GO/Ag-coated NiTi alloy substrates of coating time. \* denotes the significant difference ( $P < 0.001$ ) from GO5 and GO10. # denotes significant difference ( $P < 0.001$ ) from GOAg5 and GOAg10.

#### 4.7 Results of Biocompatibility Testing

Biocompatibility of the GO and the GO/Ag coatings were assessed from MTT assay which measures the change of a yellow water-soluble MTT dye into a purple formazan crystal formed by active mitochondria [133]. The microscopy images of the cells while seeding is shown in Figure 24 and after incubating 24 h in conditioned medium is shown in Figure 25 for the bare NiTi alloy, the GO-coated and the GO/Ag-coated NiTi alloy substrates. Figure 26 shows the number of viable cells (human

gingival fibroblasts) after incubating 24 h in conditioned medium from the bare NiTi alloy, the GO-coated and the GO/Ag-coated NiTi alloy substrates.

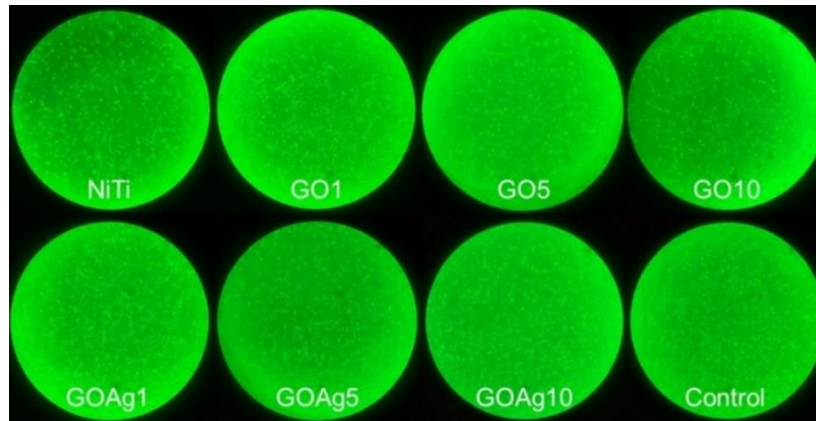


Figure 24 Microscopy images (20x) of cells (gingival fibroblasts) while seeding of cells of the bare NiTi alloy, the GO-coated (GO1, GO5, GO10), and the GO/Ag-coated (GOAg1, GOAg5, GOAg10) NiTi alloy substrates.

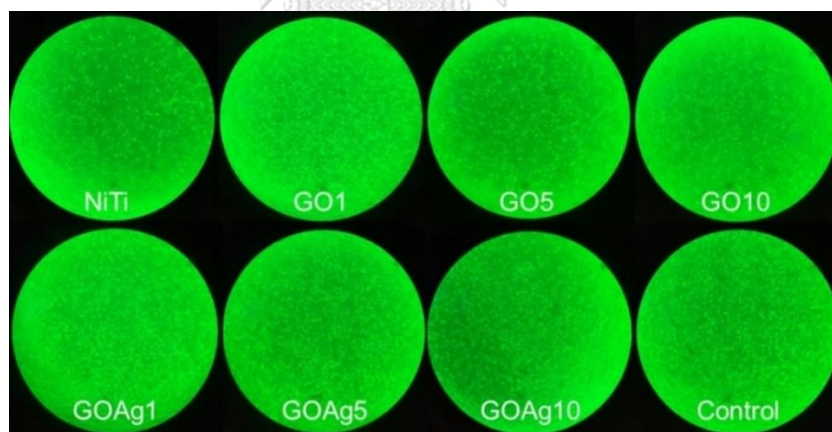


Figure 25 Microscopy images (20x) of cells (gingival fibroblasts) after incubating 24 h with conditioned medium of the bare NiTi alloy, the GO-coated (GO1, GO5, GO10), and the GO/Ag-coated (GOAg1, GOAg5, GOAg10) NiTi alloy substrates.

The mean results of three independent experiments and shown as mean  $\pm$  SD (Figure 26). Bare NiTi group presented significantly lower viable cells compared to GO-

coated, GO/Ag-coated NiTi substrates and control group ( $P < 0.05$ ). This may be because of release of Ni and Ti from bare NiTi alloy and the ions were more cytotoxic to human gingival fibroblasts. There was no significant difference of the viable cells of GO10 ( $P = 0.238$ ) and GOAg10 ( $P = 0.503$ ) from control which may be because of the presence of thicker protective coatings and less release of Ni and Ti ions compared to 1 min and 5 min coatings.

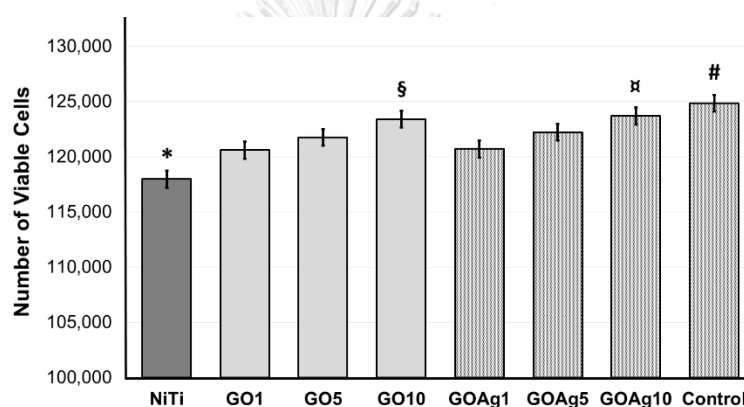


Figure 26 Number of viable cells (gingival fibroblasts) after incubating 24 h in conditioned medium of the bare NiTi alloy, the GO-coated (GO1, GO5, GO10), and the GO/Ag-coated (GOAg1, GOAg5, GOAg10) NiTi alloy substrates and the control (cells incubated with growth medium). The data were obtained from three independent experiments and shown as mean  $\pm$  SD. \* denotes significant different ( $P < 0.001$ ) from GO-coated (GO1, GO5, GO10), the GO/Ag coated (GOAg1, GOAg5, GOAg10) and the control. § denotes the significant difference compared to the GO1 and bare NiTi alloy ( $P < 0.05$ ). α denotes the significant difference compared to the GOAg1 and bare NiTi alloy ( $P < 0.05$ ). # denotes the significant difference compared to the GO1, GO5, GOAg1, GOAg5 and bare NiTi alloy ( $P < 0.05$ ).

Furthermore, in GO-coated groups, GO10 showed significantly higher viable cells compared to GO1 ( $P = 0.02$ ), and in GO/Ag-coated groups, GOAg10 showed

significantly higher viable cells compared to GOAg1 ( $P = 0.001$ ) which is due to thinner coatings in 1 min and more release of Ni and Ti ions where were more cytotoxic to gingival fibroblasts.



## CHAPTER V

### DISCUSSION

For various applications, graphene-based materials have been used to coat various metallic substrates [117, 134]. Following parts present the discussion of this research findings in various aspects.

#### 5.1 Surface Characterization of the Coatings

Common forms of carbon include: crystalline (diamond, graphite, and fullerenes), disordered (glassy carbon, nanocrystalline carbon, graphitic amorphous carbon, diamond-like amorphous carbon, tetrahedral amorphous carbon, and diamond-like or polymer-like hydrogenated amorphous carbon), or molecular (fullerene, graphene and related materials) [135]. Graphene and GO consist of carbon atoms creating a 2D hexagonal lattice with oxygenated functionalities, such as the carboxylic acid, and hydroxyl and epoxy group [12].

The Raman spectrum of graphene shows a distinct D band at approx.  $1,300\text{ cm}^{-1}$  and a G band at approx.  $1,600\text{ cm}^{-1}$  [86, 87]. Ferrari and Robertson suggested that the G and D peaks are due to  $sp^2$  only and this mode is forbidden in perfect graphite [136]. Diamond has a single Raman active mode at  $1332\text{ cm}^{-1}$ , which is a zone center

mode of  $T_{2g}$  symmetry [137]. Similarly, the Raman spectra of other forms of carbon is different from that of the graphene and GO [87]. In this study, the Raman spectra of the both GO-coated and GO/Ag-coated NiTi substrates show D and G bands and confirms that the carbon compound coated on NiTi alloy using EPD is in fact graphene and not another form of carbon. A high  $I_D/I_G$  ratio indicates defects in the graphitic materials, suggesting an adequate oxidation of graphite into graphite oxide [86, 117].

In our study, we used trisodium citrate, a reducing and stabilizing agent, to reduce  $AgNO_3$  to AgNPs. Raman spectra helped to confirmed that GO was not reduced to rGO as surface morphology, electrical, thermal and mechanical properties are similar. A study by Singh et al. [86] found that the Raman spectra of the  $I_D/I_G$  ratio of GO composite coating of 0.85 (D and G bands at  $1353\text{ cm}^{-1}$  and  $1591\text{ cm}^{-1}$ , respectively), whereas, the Raman spectra of the  $I_D/I_G$  ratio of rGO composite coating of 0.937 (D and G bands at  $1353\text{ cm}^{-1}$  and  $1584\text{ cm}^{-1}$ , respectively). Similarly, another study also found that the  $I_D/I_G$  ratio of GO to be 0.81 and rGO to be 0.98 [78]. Vi *et al.* [138] also mention that the  $I_D/I_G$  ratio of GO to be 0.85 which is close to our study. In our study, the  $I_D/I_G$  ratios for GO and GO/Ag coated samples showed 0.83 which is close GO rather than rGO. This confirmed that in our study, the graphene is in oxide form (GO).

In our study, the surface structure of the GO-coated and the GO/Ag-coated NiTi alloys was homogeneous with some voids and no cracks. In addition, the GO/Ag-coated NiTi alloys showed the presence of Ag in the GO/Ag coatings in EDS analysis shows.

The Ag content increased with coating time due to the increase in the thickness of the GO/Ag coatings. It has always been a challenge to create a precise uniform graphene coating using EPD because the GO coatings are always non-dense, but homogenous with some porosities [97, 139].

## 5.2 Coatings Thickness and Surface Roughness

The surface roughness is an important to determine the adhesion of the coating and coverage on the substrate. Coatings on TiN films on steel substrates with a poor surface finish show poorer adhesion than on those with a smooth surface [140]. In our study, the thickness of the GO coatings ranged from 0.34 to 1.12  $\mu\text{m}$  and for GO/Ag coatings ranged from 0.45 to 1.33  $\mu\text{m}$ . In addition, it shows that the thickness of the GO and GO/Ag coating increased with the increased coating time. In the literature, it has been mentioned that the thickness of single-layer graphene and GO can be found within the range of 0.5 to 2 nm [141]. Therefore, this indicates that the coatings developed in our study are multilayer.

In our study, the surface roughness ( $R_a$ ) of the GO and GO/Ag coatings increased with an increase in the coating time. The  $R_a$  of the GO-coated and GO/Ag-coated NiTi substrates was higher than that of the bare NiTi alloys, which indicates the presence of graphene coatings on NiTi alloy. The surface roughness of the GO and GO/Ag coatings was due to the stacking of the graphene layers formed during the electrodeposition.



Our finding corresponds to the study by Raza *et al.*[117] where a GO coating was applied to copper using EPD. The much lower roughness in their study could be due to the use of a lower voltage (<15 V) as compared to the high voltage (30 V) used in our study. The increase in voltage during EPD increases the GO thickness and the stacking of the GO layers, and thus increases the Ra of the coating [117, 142].

### 5.3 Friction Coefficient of the Coatings

The friction behavior of graphene and GO has been investigated over the last few years. Adding GO in water-based lubricants reduced steel plate friction coefficient (0.05) with no apparent surface wear [104]. Berman *et al.* [105] used a graphene coating on steel, and Lin *et al.* [95] used a graphene platelet coating to reduce the friction on load carrying machines and found that graphene significantly reduced the friction. Increasing the coating time influences the mechanical and tribological properties of graphene due to more graphene sheets. There are several explanations for the low friction of graphene related materials [77].

The friction behavior of graphene depends on the stacking, structural features, and nature of the sliding surfaces [77]. The low friction of graphene based materials is due to the interlayer graphene interactions causing wrinkling, the weak bonding between the basal planes, leading to increased lubrication [77, 143]; or due to the intrinsic graphene properties [121]. In our study, increasing coating time from 1–10 min,

increased the coating thickness, but reduced the friction coefficient which might be due to combinations of the above reasons. The coating thickness might play a major role in reducing the friction. Biomaterials with these characteristics would be beneficial to use in dental and medical applications.

#### 5.4 Hardness and Modulus of Elasticity of the Coated NiTi Alloy

In our study, in both the GO-coated and the GO/Ag-coated groups, the hardness decreased with increasing coating time from 1 min to 10 min. This might be due to the increase in the interlayer spacing between the graphene layers. In contrast, the modulus of elasticity of the GO-coated and the GO/Ag-coated groups increased with increased coating time from 1 to 10 min, which might be due to increased coating thickness leading to increased stiffness. Hence, thinner graphene coating showed better elastic recovery from load application.



#### 5.5 Surface Adhesion Properties of the Coatings

The surface adhesion properties including adhesion force and energy are important properties of the surface coating used in graphene-based materials for various applications. These determine the stability of the coatings on the substrates for different applications (such as friction reduction, protective coating, and biomedical

applications). AFM in the tapping mode was used to investigate the surface properties of graphene on various substrates [122, 141].

In our study, the surface adhesion force and energy of the GO-coated and GO/Ag-coated NiTi alloy substrates showed a non-linear pattern which might be due to the non-uniform coating. The reason for the high surface adhesion force and energy in 1 min coating might be due to the thin GO coating layer compared with that of 5 min and 10 min coatings. In addition, the adhesion forces of GO-coated in our study are lower than the finding by Ding *et al.*[141] who reported an adhesion force of 66.3 nN for the surface of a graphene nanosheet, and 170.6 nN for the surface of a GO nanosheet.

In our study, however, it was shown that the adhesion force and energy are less correlated with the coating roughness or coating thickness. This signifies that the GO layer bonds well to the NiTi substrate irrespective of the thickness of the GO layers or the roughness of the GO coatings on the NiTi alloy. The adhesion force is related to the contact angle and hydrophobicity of the substrate. A reduced area of contact decreases the adhesive force of the GO-coated substrates. Liang *et al.*[122] claimed that the adhesion of GO films has a linear relationship with the applied voltage and film thickness on a Si substrate. They mentioned that the higher the voltage applied, the thicker the film will be, which causes an increase in the adhesion owing to a stronger influence at a higher working voltage. In addition, the results of adhesion

energy of GO and GO/Ag coatings on NiTi alloy comparable with the results obtained by Jiang *et al.*[96] who measured the adhesion energies of monolayer graphene using a method similar to our own with an AFM microscope tip, and found adhesion energies of 0.46 J/m<sup>2</sup> and 0.75 J/m<sup>2</sup> for monolayer graphene on SiO<sub>2</sub> and Cu, respectively. They mentioned that the adhesion energy is related to the interfacial tension; however, in our study, we did not consider the surface tension.

In addition, Das *et al.*[100] found slightly higher adhesion energy than in our study. In their study, they found a higher adhesion energy (6 times) of graphene on Ni than on Cu (Ni, 72.7 J/m<sup>2</sup>; Cu, 12.8 J/m<sup>2</sup>). They mentioned that this may be due to the Ni interface exhibiting more covalent bonding than graphene and Cu, which is partially ionic. The reason for their higher adhesion energy than that determined in our study might be due to the different testing method and substrates used; they applied a nano-scratch test on Ni and Cu substrates. In addition, Ti has less separation than other metals such as Co, Ru, Cu, Pd, Pt, and Ag. Lattice matching also plays an important role in determining the interface structure. Zhao *et al.* [97] described the basic absorption models of graphene on hexagonally arranged metal surfaces. There is only one single adsorption site for carbon atoms on Ni and Co substrates owing to the good lattice match, yielding strong interactions.

## 5.6 Biocompatibility of the Coatings

Graphene and graphene oxide are possible candidates for biomedical applications, such as cell labeling, bacterial inhibition, anticancer drug formulations and drug delivery [144]. Hence, cytotoxicity evaluation of graphene-based materials is an important aspect. MTT assay also evaluates cell-biomaterial interaction and relates to the number of viable cells [133, 145]. This colorimetric method is an economical, accurate and reliable method for cytotoxicity determination [146, 147]. In our study, we did MTT assay to determine biocompatibility of the GO-coated and GO/Ag-coated NiTi alloys and it was found that both coatings were non-toxic to the human gingival fibroblasts.

GO coatings have used as biocompatible coatings to improve to improve hemocompatibility. Example of such coatings includes GO with chitosan [144], bovine serum albumin and heparin [148]. Liao et al. [144] mentioned that the toxicity of graphene and GO depends on the exposure environment (whether or not aggregation occurs) and mode of interaction with cells (adherent cells or suspension). Biopolymer GO coatings were also less toxic to red blood cells due electrostatic repulsions between GO and red blood cells [148]. In our study, we used low concentration (0.01 mg/ml concentration of GO), hence the GO coatings were non-toxic to gingival fibroblasts.

Suarez-Martinez *et al.* mentioned that transition metals improve the mechanical properties of GO coatings [149]. AgNPs interact with each other and form a triangular lattice by donating 1–2 electrons to the graphene [150]. Our pilot study demonstrated that AgNPs do not adhere well on a Ni–Ti alloy substrate without GO as a carrier. Another major advantage of the GO/Ag nanocomposite coating in our research is its antibacterial actions. GO/Ag nanocomposites have strong antibacterial actions against gram-negative bacteria *E. coli* compared with the original AgNPs [23, 151]. This suggests that nanocomposites coatings may be used as an effective antibacterial coating in addition to its protective effect.

Within our limitations, in this study, NiTi alloys were successfully coated GO and the GO/Ag nanocomposite coatings. The GO-coated and the GO/Ag-coated NiTi alloys showed good surface properties. In addition, GO-coated and GO/Ag-coated NiTi alloy substrates were non-toxic to human gingival fibroblasts, hence, these coatings can be used as biocompatible protective coatings for biomedical applications. Further studies can be done to study the effects of the contact angle, hydrophobicity, and surface tension on the adhesion properties of the GO and GO/Ag coatings on NiTi alloys.

## CHAPTER VI

### CONCLUSION

The GO and the GO/Ag coatings were successfully developed on NiTi alloys with varying the coating time using the electrophoretic deposition and the coatings were confirmed from the Raman spectra. The coating thickness and the surface roughness increased with an increase in coating time from 1 to 10 min. The GO-coated and GO/Ag-coated NiTi alloy demonstrated improved mechanical strength and a reduced friction coefficient than the bare NiTi alloys. The GO and the GO/Ag coatings on NiTi alloy have a good surface adhesion. A strong positive correlation was found between the adhesion force and energy of the coatings on NiTi alloys.

Both the GO-coated and the GO/Ag-coated NiTi alloy can be used for various dental nanocomposite materials for biomedical applications.

## APPENDIX



No. 103/2018

### Study Protocol and Consent Form Approval

The Human Research Ethics Committee of the Faculty of Dentistry, Chulalongkorn University, Bangkok, Thailand has approved the following study to be carried out according to the protocol and patient/participant information sheet dated and/or amended as follows in compliance with the **ICH/GCP**

**Study Title** : Development of grapheme oxide/Silver (GO/ Ag) nanocomposite coating on NiTi alloy for biomedical applications

**Study Code** : HREC-DCU 2018-084

**Study Center** : Chulalongkorn University

**Principle Investigator** : Mr. Dinesh Rokaya

**Protocol Date** : August 10, 2018

**Date of Approval** : October 30, 2018

**Date of Expiration** : October 29, 2020

(Associate Professor Dr. Veera Lertchirakarn)  
**Chairman of Ethics Committee**

(Assistant Professor Dr. Kanokporn Bhalang)  
**Associate Dean for Research**

\*A list of the Ethics Committee members (names and positions) present at the Ethics Committee meeting on the date of approval of this study has been attached (upon requested). This Study Protocol Approval Form will be forwarded to the Principal Investigator.

Approval is granted subject to the following conditions: (see back of the approval)



Figure A1. Ethical Approval Document 1.

All approved investigators must comply with the following conditions:

1. Strictly conduct the research as required by the protocol;
2. Use only the information sheet, consent form (and recruitment materials, if any) bearing the Human Research Ethics Committee's seal of approval ; and return one copy of such documents of the first subject recruited to the Human Research Ethics Committee for the record;
3. Report to the Human Research Ethics Committee any serious adverse event or any changes in the research activity within five working days;
4. Provide reports to the Human Research Ethics Committee concerning the progress of the research upon the specified period of time or when requested;
5. If the study cannot be finished within the expire date of the approval certificate, the investigator is obliged to reapply for approval at least one month before the date of expiration.

นักวิจัยทุกท่านที่ผ่านการรับรองจริยธรรมการวิจัยต้องปฏิบัติตามดังต่อไปนี้

1. ดำเนินการวิจัยตามที่ระบุไว้ในโครงการวิจัยอย่างเคร่งครัด
2. ใช้เอกสารแนะนำอาสาสมัคร ใบยินยอม (และเอกสารเชิญเข้าร่วมวิจัยหรือใบโฆษณาถ้ามี) เฉพาะที่มีตราประทับของคณะกรรมการพิจารณาจริยธรรมการวิจัยเท่านั้น และส่งสำเนาเอกสารดังกล่าวที่ใช้กับผู้เข้าร่วมวิจัยจริงรายแรกมาที่สำนักงานคณะกรรมการพิจารณาจริยธรรมการวิจัย คณะทันตแพทยศาสตร์ เพื่อเก็บไว้เป็นหลักฐาน
3. รายงานเหตุการณ์ไม่พึงประสงค์ร้ายแรงที่เกิดขึ้นหรือการเปลี่ยนแปลงกิจกรรมวิจัยใดๆ ต่อคณะกรรมการพิจารณาจริยธรรมการวิจัย ภายใน 5 วันทำการ
4. ส่งรายงานความก้าวหน้าต่อคณะกรรมการพิจารณาจริยธรรมการวิจัย ตามเวลาที่กำหนดหรือเมื่อได้รับการร้องขอ
5. หากการวิจัยไม่สามารถดำเนินการเสร็จสิ้นภายในกำหนด ผู้วิจัยต้องยื่นขออนุมัติใหม่ก่อนวันสิ้นสุดการอนุมัติอย่างน้อย 1 เดือน

Figure A2. Ethical Approval Document 2.

**Table A1** Results of descriptive statistics of EDS analysis (C and O) of the bare NiTi and coated NiTi alloy substrates.

	N	Mean	Std. Deviation	Std. Error	95% CI for Mean		Min	Max
					Lower Bound	Upper Bound		
C GO1	3	10.980	.257	.148	10.341	11.618	10.78	11.27
GO5	3	12.566	.272	.157	11.890	13.242	12.39	12.88
GO10	3	14.390	.278	.160	13.697	15.082	14.16	14.70
GOAg1	3	5.723	1.218	.703	2.697	8.749	5.02	7.13
GOAg5	3	6.350	1.160	.670	3.467	9.232	5.68	7.69
GOAg10	3	8.923	.750	.433	7.058	10.787	8.49	9.79
NiTi	3	1.863	1.322	.763	-1.421	5.147	1.10	3.39
Total	21	8.685	4.194	.915	6.776	10.594	1.10	14.70
O GO1	3	1.643	.321	.185	.844	2.441	1.41	2.01
GO5	3	4.226	.479	.276	3.035	5.418	3.93	4.78
GO10	3	5.000	.157	.090	4.609	5.390	4.82	5.11
GOAg1	3	5.873	2.471	1.426	-.265	12.011	3.02	7.30
GOAg5	3	8.490	3.481	2.010	-.158	17.138	4.47	10.50
GOAg10	3	10.226	4.283	2.473	-.415	20.868	5.28	12.70
NiTi	3	2.960	.762	.440	1.066	4.853	2.08	3.40
Total	21	5.488	3.456	.754	3.915	7.061	1.41	12.70

C= Carbon, O= oxygen, SD= Standard deviation, Std = Standard, CI= Confidence interval, Min= Minimum and Max= Maximum.

**Table A2** Results of descriptive statistics of EDS analysis (Ti, Ni and Ag) of the bare NiTi and coated NiTi alloy substrates.

	N	Mean	SD	Std. Error	95% CI for Mean		Min	Max	
					Lower Bound	Upper Bound			
Ti	GO1	3	39.870	.278	.160	39.178	40.561	39.62	40.17
	GO5	3	38.503	.498	.288	37.263	39.742	38.13	39.07
	GO10	3	36.123	.470	.271	34.953	37.292	35.58	36.41
	GOAg1	3	35.473	1.010	.583	32.963	37.983	34.89	36.64
	GOAg5	3	32.846	.444	.256	31.742	33.951	32.59	33.36
	GOAg10	3	29.343	2.447	1.413	23.262	35.424	27.93	32.17
	NiTi	3	49.803	7.095	4.096	32.176	67.429	41.61	53.90
Ni	GO1	3	47.506	.835	.482	45.432	49.581	46.55	48.09
	GO5	3	44.703	.869	.501	42.543	46.863	43.72	45.37
	GO10	3	44.486	.690	.398	42.771	46.201	43.81	45.19
	GOAg1	3	38.250	3.325	1.920	29.988	46.511	36.33	42.09
	GOAg5	3	34.216	3.787	2.186	24.808	43.625	32.03	38.59
	GOAg10	3	31.133	2.811	1.623	24.148	38.118	29.51	34.38
	NiTi	3	45.373	6.535	3.773	29.138	61.608	41.60	52.92
Ag	GOAg1	3	14.680	3.083	1.780	7.021	22.338	11.12	16.46
	GOAg5	3	18.096	1.911	1.103	13.349	22.843	15.89	19.20
	GOAg10	3	20.373	1.726	.996	16.085	24.661	18.38	21.37

Ti = Titanium, Ni = Nickel, Ag = Silver, SD= Standard deviation, Std = Standard, CI= Confidence interval, Min= Minimum and Max= Maximum

**Table A3** Results of descriptive statistics of coating thickness on NiTi alloy and roughness of the bare and coated NiTi alloy substrates.

	N	Mean	SD	Std. Error	95% Confidence Interval		Min	Max	
					Lower Bound	Upper Bound			
Thickness ( $\mu\text{m}$ )	GO1	5	.344	.143	.064	.165	.522	.16	.50
	GO5	5	.651	.107	.048	.518	.785	.52	.79
	GO10	5	1.327	.095	.042	1.209	1.445	1.18	1.43
	GOAg1	6	.482	.063	.026	.415	.549	.39	.57
	GOAg5	6	.763	.281	.115	.467	1.059	.56	1.13
	GOAg10	6	1.385	.097	.039	1.283	1.488	1.27	1.53
	Total	33	.830	.426	.074	.679	.981	.16	1.53
Roughness (Ra)	GO1	10	49.928	9.113	2.88	43.409	56.447	39.87	63.13
	GO5	10	63.449	3.779	1.195	60.745	66.153	55.15	68.63
	GO10	10	66.558	4.246	1.342	63.520	69.596	60.56	72.64
	GOAg1	10	52.284	11.589	3.664	43.994	60.575	41.69	71.65
	GOAg5	10	64.511	3.969	1.255	61.672	67.351	60.01	71.65
	GOAg10	10	68.033	3.168	1.001	65.767	70.300	63.13	72.44
	NiTi	10	32.450	4.063	1.285	29.543	35.356	28.43	41.84
	Total	70	56.745	13.450	1.607	53.537	59.952	28.43	72.64

SD= Standard deviation, Std = Standard, CI= Confidence interval, Min= Minimum and Max= Maximum

**Table A4** Multiple comparison of GO coating thickness ( $\mu\text{m}$ ) on NiTi alloy substrates.

(I) Type	(J) Type	Mean Difference (I-J)	Std. Error	Sig.	95% Confidence Interval	
					Lower Bound	Upper Bound
GO1	GO5	-.307*	.074	.005	-.514	-.101
	GO10	-.983*	.074	.000	-1.19	-.776
GO5	GO1	.307*	.074	.005	.101	.514
	GO10	-.675*	.074	.000	-.882	-.469
GO10	GO1	.983*	.074	.000	.776	1.19
	GO5	.675*	.074	.000	.469	.882

\*. The mean difference is significant at the 0.05 level.



**Table A5** Multiple comparison showing subset of GO coating thickness on NiTi alloy.

Type	N	Subset for alpha = 0.05		
		1	2	3
GO1	5	.344		
GO5	5		.651	
GO10	5			1.327
Sig.		1	1	1

Means for groups in homogeneous subsets are displayed.

**Table A6** Multiple comparison of GO/Ag coating thickness ( $\mu\text{m}$ ) on NiTi alloy substrates.

(I) Type	(J) Type	Mean Difference (I-J)	Std. Error	Sig.	95% Confidence Interval	
					Lower Bound	Upper Bound
GO1	GO5	-.307*	.074	.005	-.514	-.101
	GO10	-.983*	.074	.000	-1.19	-.776
GO5	GO1	.307*	.074	.005	.101	.514
	GO10	-.675*	.074	.000	-.882	-.469
GO10	GO1	.983*	.074	.000	.776	1.19
	GO5	.675*	.074	.000	.469	.882

\*. The mean difference is significant at the 0.05 level.

**Table A7** Multiple comparison showing subset of GO/Ag coating thickness on NiTi alloy.

Type	N	Subset for alpha = 0.05		
		1	2	3
GO1	5	.344		
GO5	5		.651	
GO10	5			1.327
Sig.		1	1	1

Means for groups in homogeneous subsets are displayed.

**Table A8** Multiple comparison of surface roughness of the GO-coated and bare NiTi alloys.

(I) Type	(J) Type	Mean Difference (I-J)	Std. Error	Sig.	95% Confidence Interval	
					Lower Bound	Upper Bound
GO1	GO5	-13.520*	2.567	.000	-21.05	-5.99
	GO10	-16.629*	2.567	.000	-24.159	-9.099
	Bare NiTi	17.478*	2.567	.000	9.948	25.008
GO5	GO1	13.520*	2.567	.000	5.99	21.05
	GO10	-3.108	2.567	.692	-10.639	4.421
	Bare NiTi	30.999*	2.567	.000	23.469	38.529
GO10	GO1	16.629*	2.567	.000	9.099	24.159
	GO5	3.108	2.567	.692	-4.421	10.639
	Bare NiTi	34.108*	2.567	.000	26.577	41.638
Bare NiTi	GO1	-17.478*	2.567	.000	-25.008	-9.948
	GO5	-30.999*	2.567	.000	-38.529	-23.469
	GO10	-34.108*	2.567	.000	-41.638	-26.577

\*. The mean difference is significant at the 0.05 level.

**Table A9** Multiple comparison showing subset of surface roughness of the bare and the GO-coated NiTi alloys.

Type	N	Subset for alpha = 0.05		
		1	2	3
NiTi	10	32.45		
GO1	10		49.928	
GO5	10			63.449
GO10	10			66.558
Sig.		1	1	.692

Means for groups in homogeneous subsets are displayed.





**Table A10** Multiple comparison of surface roughness of the GO/Ag coated NiTi and bare alloys.

(I) Type	(J) Type	Mean Difference (I-J)	Std. Error	Sig.	95% Confidence Interval	
					Lower Bound	Upper Bound
GOAg1	GOAg5	-12.227*	2.971	.003	-20.94	-3.512
	GOAg10	-15.748*	2.971	.000	-24.463	-7.034
	NiTi	19.834*	2.971	.000	11.12	28.549
GOAg5	GOAg1	12.227*	2.971	.003	3.512	20.941
	GOAg10	-3.521	2.971	.706	-12.236	5.192
	NiTi	32.061*	2.971	.000	23.347	40.776
GOAg10	GOAg1	15.748*	2.971	.000	7.034	24.463
	GOAg5	3.521	2.971	.706	-5.192	12.236
	NiTi	35.583*	2.971	.000	26.869	44.297
NiTi	GOAg1	-19.834*	2.971	.000	-28.549	-11.12
	GOAg5	-32.061*	2.971	.000	-40.776	-23.347
	GOAg10	-35.583*	2.971	.000	-44.297	-26.86

\*. The mean difference is significant at the 0.05 level.

**Table A11** Multiple comparison showing subset of surface roughness of the bare and the GO/Ag-coated NiTi alloys.

Type	N	Subset for alpha = 0.05		
		1	2	3
NiTi	10	32.45		
GOAg1	10		52.284	
GOAg5	10			64.511
GOAg10	10			68.033
Sig.		1	1	.706

Means for groups in homogeneous subsets are displayed.



**Table A12** Results of descriptive statistics of hardness and modulus of elasticity of the

	N	Mean	SD	Std. Error	95% CI for Mean		Min	Max	
					Lower Bound	Upper Bound			
Hardness (GPa)	GO1	6	.884	.099	.04	.780	.988	.697	.978
	GO5	6	.395	.12	.049	.269	.521	.241	.598
	GO10	6	.414	.09	.036	.319	.508	.312	.523
	GOAg1	6	.923	.15	.061	.765	1.080	.814	1.212
	GOAg5	6	.433	.117	.048	.310	.556	.235	.563
	GOAg10	6	.445	.077	.031	.363	.526	.346	.543
	Total	36	.582	.253	.042	.496	.668	.235	1.212
Modulus of Elasticity (GPa)	GO1	6	1.138	.188	.076	.941	1.336	.936	1.328
	GO5	6	3.514	.473	.193	3.016	4.011	3.083	4.108
	GO10	6	4.251	.692	.282	3.524	4.977	3.620	5.132
	GOAg1	6	1.153	.195	.079	.948	1.357	.905	1.365
	GOAg5	6	4.282	.742	.303	3.503	5.061	3.167	5.326
	GOAg10	6	4.896	.441	.18	4.433	5.360	4.314	5.307
	Total	36	3.206	1.6	.266	2.664	3.747	.905	5.326

GO-coated and GO/Ag-coated NiTi alloys.

SD= Standard deviation, Std = Standard, CI= Confidence interval, Min= Minimum and Max= Maximum

**Table A13** Results of multiple comparison of hardness of the GO-coated NiTi alloys.

(I) Type	(J) Type	Mean Difference (I-J)	Std. Error	Sig.	95% Confidence Interval	
					Lower Bound	Upper Bound
GO1	GO5	.4890*	.06	.000	.326	.651
	GO10	.4705*	.06	.000	.307	.633
GO5	GO1	-.489*	.06	.000	-.651	-.326
	GO10	-.0185	.06	.954	-.181	.144
GO10	GO1	-.4705*	.06	.000	-.633	-.307
	GO5	.0185	.06	.954	-.144	.181

\*. The mean difference is significant at the 0.05 level.



**Table A14** Multiple comparison showing subset of hardness of the GO-coated NiTi alloys.

Type	N	Subset for alpha = 0.05	
		1	2
GO5	6	.395	
GO10	6	.414	
GO1	6		.884
Sig.		.954	1

Means for groups in homogeneous subsets are displayed.

**Table A15** Results of multiple comparison of hardness of the GO/Ag-coated NiTi alloys.

(I) Type	(J) Type	Mean Difference (I-J)	Std. Error	Sig.	95% Confidence Interval	
					Lower Bound	Upper Bound
GOAg1	GOAg5	.489*	.068	.000	.303	.675
	GOAg10	.478*	.068	.000	.292	.664
GOAg5	GOAg1	-.489*	.068	.000	-.675	-.303
	GOAg10	-.011	.068	.986	-.197	.174
GOAg10	GOAg1	-.478*	.068	.000	-.664	-.292
	GOAg5	.0115	.068	.986	-.174	.197

\*. The mean difference is significant at the 0.05 level.

**Table A16** Multiple comparison showing subset of hardness of the GO/Ag-coated NiTi alloys.

Type	N	Subset for alpha = 0.05	
		1	2
GOAg5	6	.433	
GOAg10	6	.445	
GOAg1	6		.923
Sig.		.986	1

Means for groups in homogeneous subsets are displayed.

**Table A17** Multiple comparison of modulus of elasticity of the GO-coated NiTi alloys.

(I) Type	(J) Type	Mean Difference (I-J)	Std. Error	Sig.	95% Confidence Interval	
					Lower Bound	Upper Bound
GO1	GO5	-2.375*	.286	.000	-3.152	-1.597
	GO10	-3.112*	.286	.000	-3.889	-2.334
GO5	GO1	2.375*	.286	.000	1.597	3.152
	GO10	-.737	.286	.065	-1.514	.04
GO10	GO1	3.112*	.286	.000	2.334	3.889
	GO5	.737	.286	.065	-.04	1.514

\*. The mean difference is significant at the 0.05 level.

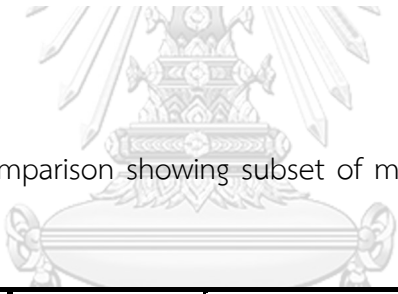


**Table A18** Multiple comparison showing subset of modulus of elasticity of the GO-coated NiTi alloys.

Type	N	Subset for alpha = 0.05	
		1	2
GO1	6	1.138	
GO5	6		3.514
GO10	6		4.251
Sig.		1	.065

Means for groups in homogeneous subsets are displayed.

**Table A19** Multiple comparison of modulus elasticity of the GO/Ag-coated NiTi alloys.

(I) Type	(J) Type	Mean Difference (I-J)	Std. Error	Sig.	95% Confidence Interval	
					Lower Bound	Upper Bound
GOAg1	GOAg5	-3.1293*	.295	.000	-3.93	-2.328
	GOAg10	-3.743*	.295	.000	-4.544	-2.942
GOAg5	GOAg1	3.129*	.295	.000	2.328	3.93
	GOAg10	-.614	.295	.149	-1.415	.186
GOAg10	GOAg1	3.743*	.295	.000	2.942	4.544
	GOAg5	.614	.295	.149	-.186	1.415

\*. The mean difference is significant at the 0.05 level.

**Table A20** Multiple comparison showing subset of modulus of elasticity of the GO/Ag-coated NiTi alloys.

Type	N	Subset for alpha = 0.05	
		1	2
GOAg1	6	1.153	
GOAg5	6		4.282
GOAg10	6		4.896
Sig.		1	.149

Means for groups in homogeneous subsets are displayed.

**Table A21** Results of descriptive statistics of surface adhesion force and energy of the GO-coated and GO/Ag-coated NiTi alloys.

	N	Mean	SD	Std. Error	95% CI for Mean		Min	Max	
					Lower Bound	Upper Bound			
Maximum unbinding force (nN)	GO1	20	14.863	6.989	1.562	11.592	18.134	3.0	26.4
	GO5	20	3.717	1.33	.297	3.094	4.340	2.1	8.3
	GO10	20	8.544	5.365	1.199	6.033	11.055	2.3	19.4
	GOAg1	20	15.332	4.627	1.034	13.167	17.498	8.8	24.9
	GOAg5	20	3.357	1.044	.233	2.868	3.846	1.6	5.0
	GOAg10	20	9.068	4.302	.962	7.054	11.082	1.6	15.5
	Total	120	9.147	6.465	.590	7.978	10.316	1.6	26.4
Energy (mJ/m <sup>2</sup> )	GO1	20	.692	.242	.054	.579	.805	.21	.96
	GO5	20	.228	.098	.021	.182	.274	.12	.58
	GO10	20	.533	.211	.047	.434	.632	.24	.88
	GOAg1	20	.713	.188	.042	.625	.801	.30	1.00
	GOAg5	20	.239	.102	.022	.191	.287	.11	.44
	GOAg10	20	.585	.227	.05	.478	.691	.15	.82
	Total	120	.498	.269	.024	.449	.547	.11	1.00

SD= Standard deviation, Std = Standard, CI= Confidence interval, Min= Minimum and Max= Maximum



**Table A22** Multiple comparison of surface adhesion force of the GO-coated NiTi alloys.

(I) Type	(J) Type	Mean Difference (I-J)	Std. Error	Sig.	95% Confidence Interval	
					Lower Bound	Upper Bound
GO1	GO5	11.146*	1.626	.000	7.057	15.236
	GO10	6.319*	1.626	.001	2.230	10.408
GO5	GO1	-11.146*	1.626	.000	-15.236	-7.057
	GO10	-4.827*	1.626	.017	-8.916	-.738
GO10	GO1	-6.319*	1.626	.001	-10.408	-2.230
	GO5	4.827*	1.626	.017	.738	8.916

\*. The mean difference is significant at the 0.05 level.



**Table A23** Multiple comparison showing subsets of surface adhesion force of the GO-coated NiTi alloys.

Type	N	Subset for alpha = 0.05		
		1	2	3
GO5	20	3.717		
GO10	20		8.544	
GO1	20			14.863
Sig.		1	1	1

Means for groups in homogeneous subsets are displayed.

**Table A24** Multiple comparison of surface adhesion force of the GO/Ag-coated NiTi alloys.

(I) Type	(J) Type	Mean Difference (I-J)	Std. Error	Sig.	95% Confidence Interval	
					Lower Bound	Upper Bound
GOAg1	GOAg5	11.975*	1.1693	.000	9.036	14.914
	GOAg10	6.264*	1.1693	.000	3.325	9.203
GOAg5	GOAg1	-11.975*	1.1693	.000	-14.914	-9.036
	GOAg10	-5.711*	1.1693	.000	-8.650	-2.772
GOAg10	GOAg1	-6.264*	1.1693	.000	-9.203	-3.325
	GOAg5	5.711*	1.1693	.000	2.772	8.650

\*. The mean difference is significant at the 0.05 level.



**Table A25** Multiple comparison showing subsets of surface adhesion force of the GO/Ag-coated NiTi alloys.

Type	N	Subset for alpha = 0.05		
		1	2	3
GOAg5	20	3.357		
GOAg10	20		9.068	
GOAg1	20			15.332
Sig.		1	1	1

Means for groups in homogeneous subsets are displayed.

**Table A26** Multiple comparison of surface adhesion energy of the GO/Ag-coated NiTi alloys.

(I) Type	(J) Type	Mean Difference (I-J)	Std. Error	Sig.	95% Confidence Interval	
					Lower Bound	Upper Bound
GO1	GO5	.464*	.061	.000	.31	.618
	GO10	.159*	.061	.042	.001	.313
GO5	GO1	-.464*	.061	.000	-.618	-.310
	GO10	-.305*	.061	.000	-.459	-.15
GO10	GO1	-.159*	.061	.042	-.313	-.001
	GO5	.305*	.061	.000	.15	.459

\*. The mean difference is significant at the 0.05 level.



**Table A27** Multiple comparison showing subsets of surface adhesion energy of the GO-coated NiTi alloys.

Type	N	Subset for alpha = 0.05		
		1	2	3
GO5	20	.228		
GO10	20		.533	
GO1	20			.692
Sig.		1	1	1

Means for groups in homogeneous subsets are displayed.

**Table A28** Multiple comparison of surface adhesion energy of the GO/Ag-coated NiTi alloys.

(I) Type	(J) Type	Mean Difference (I-J)	Std. Error	Sig.	95% Confidence Interval	
					Lower Bound	Upper Bound
GOAg1	GOAg5	.474*	.057	.000	.33	.617
	GOAg10	.128	.057	.090	-.015	.271
GOAg5	GOAg1	-.474*	.057	.000	-.617	-.33
	GOAg10	-.346*	.057	.000	-.489	-.202
GOAg10	GOAg1	-.128	.057	.090	-.271	.015
	GOAg5	.346*	.057	.000	.202	.489

\*. The mean difference is significant at the 0.05 level.

**Table A29** Multiple comparison showing subsets of surface adhesion energy of the GO/Ag-coated NiTi alloys.

Type	N	Subset for alpha = 0.05	
		1	2
GOAg5	20	.239	
GOAg10	20		.585
GOAg1	20		.713
Sig.		1	.090

Means for groups in homogeneous subsets are displayed.

**Table A30** Results of descriptive statistics of friction of the GO-coated and bare NiTi alloys.

	N	Mean	SD	Std. Error	95% CI for Mean		Min	Max
					Lower Bound	Upper Bound		
GO1	59	.022	.014	.001	.018	.026	.002	.040
GO5	59	.013	.011	.001	.01	.016	-.011	.036
GO10	59	.006	.005	.001	.004	.007	-.007	.020
GOAg1	59	.023	.021	.002	.018	.029	-.022	.055
GOAg5	59	.015	.013	.001	.012	.019	-.012	.035
GOAg10	59	.006	.005	.001	.005	.008	-.006	.011
NiTi	59	.061	.049	.006	.048	.073	.001	.145
Total	413	.021	.028	.001	.018	.024	-.022	.145

SD= Standard deviation, CI= Confidence interval, Min= Minimum and Max= Maximum

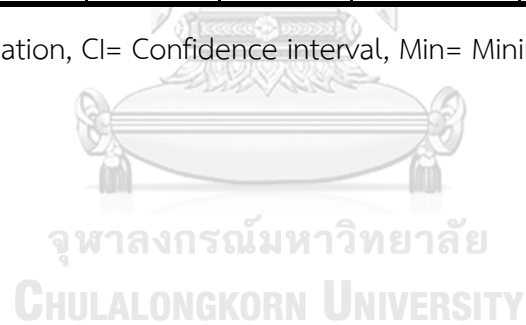


**Table A31** Multiple comparison of friction of the GO-coated and bare NiTi alloys.

(I) Substrates	(J) Substrates	Mean Difference (I-J)	Std. Error	Sig.	95% Confidence Interval	
					Lower Bound	Upper Bound
GO1	GO5	.009	.004	.532	-.005	.023
	GO10	.016*	.004	.016	.001	.031
	NiTi	-.038*	.004	.000	-.053	-.023
GO5	GO1	-.009	.004	.532	-.023	.005
	GO10	.007	.004	.809	-.007	.021
	NiTi	-.047*	.004	.000	-.062	-.033
GO10	GO1	-.016*	.004	.016	-.031	-.001
	GO5	-.007	.004	.809	-.021	.007
	NiTi	-.054*	.004	.000	-.069	-.040
NiTi	GO1	.038*	.004	.000	.023	.053
	GO5	.047*	.004	.000	.033	.062
	GO10	.054*	.004	.000	.040	.069

\*. The mean difference is significant at the 0.05 level.

Table A32 Multiple comparison of friction of the GO/Ag-coated and bare NiTi alloys.

(I) Substrates	(J) Substrates	Mean Difference (I-J)	Std. Error	Sig.	95% Confidence Interval	
					Lower Bound	Upper Bound
GOAg1	GOAg5	.007	.004	.733	-.006	.022
	GOAg10	.016*	.004	.012	.002	.031
	NiTi	-.037*	.004	.000	-.052	-.022
GOAg5	GOAg1	-.007	.004	.733	-.022	.006
	GOAg10	.008	.004	.580	-.005	.023
	NiTi	-.045*	.004	.000	-.059	-.030
GOAg10	GOAg1	-.0167*	.004	.012	-.031	-.002
	GOAg5	-.008	.004	.580	-.023	.005
	NiTi	-.054*	.004	.000	-.068	-.039
NiTi	GOAg1	.037*	.004	.000	.022	.052
	GOAg5	.045*	.004	.000	.030	.059
	GOAg10	.054*	.004	.000	.039	.068

**Table A33** Multiple comparison showing subsets of friction of bare and coated NiTi alloys.

Substrates	N	Subset for alpha = 0.05		
		1	2	3
GO10	59	.006		
GOAg10	59	.006		
GO5	59	.013	.013	
GOAg5	59	.015	.015	
GO1	59		.022	
GOAg1	59		.023	
Bare NiTi	59			.061
Sig.		.488	.399	1

Means for groups in homogeneous subsets are displayed.





**Table A34** Results of viable cells of the bare and coated NiTi alloys.

	N	Mean	SD	Std. Error	95% CI for Mean		Min	Max
					Lower Bound	Upper Bound		
Bare NiTi	3	1.179E5	1240.534	716.223	1.148E5	1.210E5	116522.2 2	118744. 44
GO1	3	1.205E5	351.774	203.097	1.197E5	1.214E5	120222.2 2	120922. 22
GO5	3	1.217E5	363.850	210.069	1.208E5	1.226E5	121333.3 3	122033. 33
GO10	3	1.233E5	184.703	106.638	1.229E5	1.238E5	123222.2 2	123588. 88
GOAg1	3	1.206E5	491.030	283.496	1.194E5	1.219E5	120255.5 5	121222. 22
GOAg5	3	1.222E5	211.694	122.222	1.216E5	1.227E5	122077.7 7	122444. 44
GOAg10	3	1.236E5	288.246	166.419	1.229E5	1.244E5	123366.6 6	123922. 22
Control	3	1.248E5	413.705	238.853	1.238E5	1.258E5	124522.2 2	125300. 00
Total	24	1.218E5	2120.334	432.811	1.209E5	1.227E5	116522.2 2	125300. 00

SD= Standard deviation, Std = Standard, CI= Confidence interval, Min= Minimum and Max= Maximum

**Table A35** Multiple comparison of viable cells of the bare and the GO-coated NiTi alloys.

(I) Groups	(J) Groups	Mean Difference (I-J)	Std. Error	Sig.	95% Confidence Interval	
					Lower Bound	Upper Bound
GO1	NiTi	2640.741*	444.347	.004	724.351	4557.131
	GO5	-1148.147	444.347	.495	-3064.536	768.242
	GO10	-2.800E3*	444.347	.002	-4716.39	-883.611
	Control	-4.237E3*	444.347	.000	-6153.427	-2320.648
GO5	NiTi	3788.888*	444.347	.000	1872.498	5705.278
	GO1	1148.147	444.347	.495	-768.242	3064.536
	GO10	-1651.854	444.347	.123	-3568.243	264.535
	Control	-3.088E3*	444.347	.001	-5005.28	-1172.501
GO10	NiTi	5440.742*	444.347	.000	3524.352	7357.132
	GO1	2800.001*	444.347	.002	883.611	4716.390
	GO5	1651.854	444.347	.123	-264.535	3568.243
	Control	-1437.037	444.347	.238	-3353.426	479.352
Control	NiTi	6877.779*	444.347	.000	4961.389	8794.169
	GO1	4237.038*	444.347	.000	2320.648	6153.427
	GO5	3088.891*	444.347	.001	1172.501	5005.28
	GO10	1437.037	444.347	.238	-479.352	3353.426

\*. The mean difference is significant at the 0.05 level.

**Table A36** Multiple comparison showing subsets of viable cells of the bare and the GO/Ag-coated NiTi alloys.

Different Groups	N	Subset for alpha = 0.05			
		1	2	3	4
NiTi	3	1.1795E5			
GO1	3		1.205E5		
GO5	3		1.217E5	1.217E5	
GO10	3			1.233E5	1.233E5
Control	3				1.248E5
Sig.		1	.356	.104	.181

Means for groups in homogeneous subsets are displayed



**Table A37** Multiple comparison showing subsets of viable cells of the bare and GO/Ag coated NiTi alloys.

(I) Groups	(J) Groups	Mean Difference (I-J)	Std. Error	Sig.	95% Confidence Interval	
					Lower Bound	Upper Bound
GOAg1	NiTi	2737.038*	444.347	.002	820.648	4653.428
	GOAg5	-1511.111	444.347	.192	-3427.5	405.278
	GOAg10	-3.000E3*	444.347	.001	-4916.389	-1083.61
	Control	-4.1407E3*	444.347	.000	-6057.13	-2224.35
GOAg5	NiTi	4248.149*	444.347	.000	2331.759	6164.539
	GOAg1	1511.111	444.347	.192	-405.278	3427.5
	GOAg10	-1488.889	444.347	.205	-3405.278	427.5
	Control	-2.6296E3*	444.347	.004	-4546.019	-713.239
GOAg10	NiTi	5737.038*	444.347	.000	3820.648	7653.428
	GOAg1	3000.000*	444.347	.001	1083.61	4916.389
	GOAg5	1488.889	444.347	.205	-427.5	3405.278
	Control	-1140.740	444.347	.503	-3057.13	775.649
Control	NiTi	6877.779*	444.347	.000	4961.389	8794.169
	GOAg1	4140.74*	444.347	.000	2224.35	6057.13
	GOAg5	2629.629*	444.347	.004	713.239	4546.019
	GOAg10	1140.740	444.347	.503	-775.649	3057.13

\*. The mean difference is significant at the 0.05 level.

**Table A38** Multiple comparison showing subsets of viable cells of the bare and the GO/Ag-coated NiTi alloys.

Different Groups	N	Subset for alpha = 0.05				
		1	2	3	4	5
NiTi	3	1.179E5				
GOAg1	3		1.206E5			
GOAg5	3		1.222E5	1.222E5	1.222E5	
GOAg10	3				1.236E5	1.236E5
Control	3					1.248E5
Sig.		1	.142	.123	.205	.238

Means for groups in homogeneous subsets are displayed.



## REFERENCES

1. Nouri A, Wen C. Introduction to surface coating and modification for metallic biomaterials. In Wen C (ed) *Surface Coating and Modification of Metallic Biomaterials*. Sydney, Australia: Elsevier Science and Technology. Woodhead Publishing Series in Biomaterials 2015; 3–60.
2. Williams D. On the nature of biomaterials. *Biomaterials* 2009; 30: 5897–5909.
3. Mihov D, Katerska B. Some biocompatible materials used in medical practice. *Trakia J Sci* 2010; 8: 119–125.
4. Hanawa T. Surface modification of metallic biomaterials. In Teoh SH (ed) *Engineering materials for biomedical applications*. Singapore: World Scientific Publishing 2004; 1–36.
5. Liu XM, Wu SL, Chu PK et al. Nano-scale surface morphology, wettability and osteoblast adhesion on nitrogen plasma-implanted NiTi shape memory alloy. *J Nanosci Nanotechnol* 2009; 9: 3449–3454.
6. Thompson SA. An overview of nickel-titanium alloys used in dentistry. *Int Endontic J* 2000; 33: 297–310.
7. Ong JL, Lucas LC. Auger electron spectroscopy and its use for the characterization of titanium and hydroxyapatite surfaces. *Biomaterials* 1998; 19: 455–464.
8. Kumar A, Khanam A, Ghafoor H. Effects of intraoral aging of arch-wires on frictional forces: An ex vivo study. *J Orthod Sci* 2016; 5: 109–116.
9. Xie D, Leng YX, Jing FJ, Huang N. A brief review of bio-tribology in cardiovascular devices. *Biosurf Biotribol* 2015; 1: 249–262.
10. Kuill T, Bhadra S, Yao D et al. Recent advances in graphene based polymer composites. *Prog Polym Sci* 2010; 35: 1350–1375.
11. Hummers WS, Offeman RE. Preparation of graphitic oxide. *J Am Chem Soc* 1958; 80: 1339.
12. Dreyer DR, Park S, Bielawski CW, Ruoff RS. The chemistry of graphene oxide. *Chem Soc Rev* 2010; 39: 228–240.

13. Li M, Liu Q, Jia Z et al. Graphene oxide/hydroxyapatite composite coatings fabricated by electrophoretic nanotechnology for biological applications. *Carbon* 2014; 67: 185–197.
14. Foo ME, Gopinath SCB. Feasibility of graphene in biomedical applications. *Biomed Pharmacother* 2017; 94: 354–361.
15. Xie H, Cao T, Rodríguez-Lozano FJ et al. Graphene for the development of the next-generation of biocomposites for dental and medical applications. *Dent Mater* 2017; 33: 765–774.
16. Rosa V, Xie H, Dubey N et al. Graphene oxide-based substrate: physical and surface characterization, cytocompatibility and differentiation potential of dental pulp stem cells. *Dent Mater* 2016; 32: 1019–1025.
17. Gong W, Hu Z, Liang Y et al. Graphene-Based Multifunctional Nanomaterials in Cancer Detection and Therapeutics. *J Nanosci Nanotechnol* 2018; 18: 5155–5170.
18. Triantou M, Todorova N, Giannakopoulou T et al. Physical Properties of Photo-Aged Graphene/Polypropylene Nanocomposites. *J Nanosci Nanotechnol* 2018; 18: 5033–5041.
19. Qin J, Yang C, Cao M et al. Two-dimensional porous sheet-like carbon-doped ZnO/g-C<sub>3</sub>N<sub>4</sub> nanocomposite with high visible-light photocatalytic performance. *Mater Lett* 2017; 189: 156–159.
20. Qin J, Zhang M, Rajendran S et al. Facile synthesis of graphene-AgVO<sub>3</sub> nanocomposite with excellent supercapacitor performance. *Mater Chem Phys* 2018; 212: 30–34.
21. Shen B, Chen S, Chen Y, Sun F. Enhancement on the tribological performance of diamond films by utilizing graphene coating as a solid lubricant. *Surf Coat Technol* 2017; 311: 35–45.
22. Szunerits S, Boukherroub R. Antibacterial activity of graphene-based materials. *J Mater Chem B* 2016; 4: 6892–6912.
23. Das MR, Sarma RK, Saikia R et al. Synthesis of silver nanoparticles in an aqueous suspension of graphene oxide sheets and its antimicrobial activity. *Colloids Surf B Biointerfaces* 2011; 83: 16–22.

24. Qin J, Zhang X, Yang C et al. Effect of Ag<sup>+</sup> and PO<sub>3</sub><sup>4-</sup> ratios on the microstructure and photocatalytic activity of Ag<sub>3</sub>PO<sub>4</sub>. *Functional Materials Letters* 2016; 9: 1650063.
25. Guo L, Yuan W, Lu Z, Li CM. Polymer/nanosilver composite coatings for antibacterial applications. *Colloids Surf A Physicochem Eng Asp* 2013; 439: 69–83.
26. Boccaccini AR, Keim S, R.Ma et al. Electrophoretic deposition of biomaterials. *J R Soc Interface* 2010; 7: S581–S613.
27. Singh BP, Jena BK, Bhattacharjee S, Besra L. Development of oxidation and corrosion resistance hydrophobic graphene oxide-polymer composite coating on copper. *Surf Coat Technol* 2013; 232: 475–481.
28. Moskalewicz T, Zych A, Łukaszczyk A et al. Electrophoretic Deposition, Microstructure, and Corrosion Resistance of Porous Sol–Gel Glass/Polyetheretherketone Coatings on the Ti-13Nb-13Zr Alloy. *Metall Trans A* 2017; 48: 2660–2673.
29. Akbulut H, Hatipoglu G, Algul H et al. Co-deposition of Cu/WC/graphene hybrid nanocomposites produced by electrophoretic deposition. *Surf Coat Technol* 2015; 284: 344–352.
30. Zeng Y, Pei X, Yang S et al. Graphene oxide/hydroxyapatite composite coatings fabricated by electrochemical deposition. *Surf Coat Technol* 2016; 286: 72–79.
31. Metoki N, Rosa CMR, Zanin H et al. Electrodeposition and biomineralization of nano-β-tricalcium phosphate on graphenated carbon nanotubes. *Surf Coat Technol* 2016; 297: 51–57.
32. FDA. Overview of medical device regulation. In *Medical Devices*. Maryland, USA: U.S. Department of Health and Human Services 2012.
33. Manivasagam G, Dhinasekaran D, Rajamanickam A. Biomedical implants. Corrosion and its prevention - a review. *Recent Pat Corros Sci* 2010; 2: 40–54.
34. Adawy A, Abdel-Fattah WI. An efficient biomimetic coating methodology for a prosthetic alloy. *Mater Sci Eng C* 2013; 33: 1813–1818.
35. Jamil H. Dental material introduction. In. Baghdad, Iraq: Dijlah University College 2016.
36. Williams D. On the mechanisms of biocompatibility. *Biomaterials* 2008; 29: 2941–2953.



37. Geetha M, Singh AK, Asokamani R, Gogia AK. Ti based biomaterials, the ultimate choice for orthopaedic implants—a review. *Prog Mater Sci* 2009; 54: 397–425.
38. Chaijaruanich A. Coating techniques for biomaterials: A review. *Chiang Mai Univ J Nat Sci* 2011; 10: 39–50.
39. Hieda J, Niinomi M, Nakai M, Cho K. Dental Materials. In *Advances in Biomaterials Science and Biomedical Applications*. Rijeka, Croatia: Intec Open Science 2013; 515–538.
40. Kim RW, Chow TW, Matinlinna JP. Ceramic dental biomaterials and CAD/CAM technology: State of the art. *J Prosthodont Res* 2014; 58: 208–216.
41. Maccauro G, Iommetti PR, Raffaelli L, Manicone PF. Alumina and Zirconia Ceramic for orthopaedic and dental devices. In Pignatello R (ed) *Biomaterials Applications for Nanomedicine*. Rijeka, Croatia: InTech 2011; 299–308.
42. Christel P, Meunier A, Dorlot JM et al. Biomechanical compatibility and design of ceramic implants for orthopedic surgery. *Ann N Y Acad Sci* 1988; 523: 234–256.
43. Liu PR, Essig ME. Panorama of dental CAD/CAM restorative systems. *Compend Contin Educ Dent* 2008; 29: 482–488.
44. Schellhammer F, Walter M, Berlis A et al. Polyethylene terephthalate and polyurethane coatings for endovascular stents: Preliminary results in canine experimental arteriovenous fistulas. *Radiology* 1999; 211: 169–175.
45. Serrano MC, Ameer GA. Recent insights into the biomedical applications of shape-memory polymers. *Macromol Biosci* 2012; 12: 1156–1171.
46. Hayashi S. Technical report on preliminary investigation of shape memory polymers. In Nagoya, Japan: Nagoya research and development center, Mitsubishi Heavy Industries Inc. 1990.
47. Behl M, Razzaq MY, Lendlein A. Multifunctional shape-memory polymers. *Adv Mater* 2010; 17: 3388–3410.
48. Shakhashiri BZ. Polymers. In *General Chemistry*. Wisconsin: Wisconsin Initiative for Science Literacy 2012; 1–5.
49. Brown S, Lemons J. Medical Applications of Titanium and Its Alloys: The material and Biological Issues. In *Special Series Publication*. West Conshohocken, PA: American Society for Testing and Materials 1996; 188.

50. Williams DF. Titanium for Medical Applications. In Brunette D, Tengvall P, Textor M (eds): Titanium in Medicine: Material science, Surface science, Engineering, Biological Responses and Medical Applications. Berlin: Germany: Springer 2001; 13–24.
51. Steinemann S. Titanium-the material of choice? *Periodontology* 2000; 17: 7–21.
52. Petrini L, Migliavacca F. Biomedical applications of shape memory alloys. *J Metall* 2011; 2011: 1–15.
53. Amini A, Cheng C. Nature of hardness evolution in nanocrystalline NiTi shape memory alloys during solid-state phase transition. *Sci Rep* 2013; 3: 2476.
54. Park JB, Kim YK. Metallic biomaterials. In Bronzino JD (ed) *The biomedical engineering handbook*, 2nd Edition. FL, USA: Boca Raton: CRC Press 2000.
55. Jani JM, Leary M, Subic A, Gibson MA. A review of shape memory alloy research, applications and opportunities. *Mater Des* 2014; 56: 1078–1113.
56. Wang Y, Ke X, Voo ZX et al. Biodegradable functional polycarbonate micelles for controlled release of amphotericin B. *Acta Biomater* 2016; 46: 211–220.
57. Wang FE, Pickart SJ, Alperin HA. Mechanism of the TiNi martensitic transformation and the crystal structures of TiNi-II and TiNi-III phases. *J Appl Phys* 1972; 43: 97–112.
58. Maetani I. Placement of self-expandable metal stents for gastric outlet obstruction. *Vid J Endosc Ency GI En* 2013; 1: 196–198.
59. Lim SG, Kim JH, Lee KM et al. Conformable covered versus uncovered self-expandable metallic stents for palliation of malignant gastroduodenal obstruction: A randomized prospective study. *Dig Liver Dis* 2014; 46: 603–608.
60. Fischer A, Wieneke H, Brauer H, Erbel R. Metallic biomaterials for coronary stents. *Z Kardiol* 2001; 90: 251–262.
61. Hanawa T, Asami K, Asaoka K. Repassivation of titanium and surface oxide film regenerated in simulated bioliquid. *J Biomed Mater Res* 1998; 40: 530–538.
62. Donachie MJ. Titanium: A technical guide. In 2nd Edition. OH, USA: ASM International 2000.
63. Adya M, Alam M, Ravindranath T et al. Corrosion in titanium dental implants: Literature review. *J Indian Prosthodont Soc* 2005; 53: 126–131.

64. Cui FZ, Luo ZS. Biomaterials modification by ion-beam processing. *Surf Coat Technol* 1999; 112: 278–285.
65. Sarkar NK, Redmond W, Schwaninger B, Goldberg AJ. The chloride corrosion behaviour of four orthodontic wires. *J Oral Rehabil* 1983; 10: 121–128.
66. Petoumenou E, Arndt M, Keilig L et al. Nickel concentration in the saliva of patients with nickel-titanium orthodontic appliances. *Am J Orthod Dentofacial Orthop* 2009; 135: 59–65.
67. Noble J, Ahing SI, Karaiskos NE, Wiltshire WA. Should I be concerned if a patient requiring orthodontic treatment has an allergy to nickel? *J Can Dent Assoc* 2008; 74: 897–898.
68. Burstone CJ, Qin B, Morton JY. NiTi archwire a new orthodontic alloy. *Am J Orthod* 1985; 87: 445–452.
69. Bravo LA, de Cabanes AG, Manero JM, Ruperez ER, Gil JF. NiTi superelastic orthodontic archwires with polyamide coating. *J Mater Sc Mater Med* 2014; 25: 555–560.
70. Gurgel JA, Pinzan-Vercelino RM, Powers J. Mechanical properties of beta-titanium wires. *Angle Orthod* 2011; 81: 471–473.
71. Geim AK, MacDonald AH. Graphene: exploring carbon flatland. *Phys Today* 2007; 60: 35–41.
72. Si Y, Samulski T. Synthesis of water soluble graphene. *Nano Lett.* 2008; 8: 1679–1682.
73. Novoselov KS, Geim AK, Morozov SV et al. Electric field effect in atomically thin carbon films. *Science* 2004; 306: 666–669.
74. Katsnelson MI. Graphene: carbon in two dimensions. *Mater Today* 2007; 10: 20–27.
75. Novoselov KS, Fal'ko VI, Colombo L et al. A roadmap for graphene. *Nature* 2012; 490: 192–200.
76. Pintoa AM, Goncalves IC, Magalhães FD. Graphene-based materials biocompatibility: A review. *Colloids Surf B* 2013; 111: 188–202.
77. Berman D, Erdemir A, Sumant AV. Graphene: a new emerging lubricant. *Mater Today* 2014; 17: 31–42.

78. Nguyen VH, Kim B-K, Jo Y-L, Shima J-J. Preparation and antibacterial activity of silver nanoparticles-decorated graphene composites. *J Supercrit Fluids* 2012; 28–35.
79. Kalita G, Ayhan ME, Sharma S et al. Low temperature deposited graphene by surface wave plasma CVD as effective oxidation resistive barrier. *Corros Sci* 2014; 78: 183–187.
80. Kirkland NT, Schiller T, Medhekar N, Birbilis N. Exploring graphene as a corrosion protection barrier. *Corros Sci* 2012; 56: 1–4.
81. Aneja KS, Böhm HLM, Khanna AS, Böhma S. Functionalised graphene as a barrier against corrosion. *FlatChem* 2017; 1: 11–19.
82. Zhao P, Shi G. Study of Poisson's Ratios of Graphene and Single-Walled Carbon Nanotubes Based on an Improved Molecular Structural Mechanics Model. *Comput Mater Con* 2011; 22: 147–168.
83. Stankovich S, Dikin DA, Dommett GHB et al. Graphene-based composite materials. *Nature* 2006; 442: 282–286.
84. Tong Y, Bohm S, Song M. Graphene based materials and their composites as coatings. *Austin J Nanomed Nanotechnol* 2013; 1: 1003.
85. Algraffee H, Borumand F, Cascarini L. Peri-implantitis. *Br J Oral Maxillofac Surg* 2012; 50: 689–694.
86. Singh BP, Nayak S, Nanda KK et al. The production of a corrosion resistant graphene reinforced composite coating on copper by electrophoretic deposition. *Carbon* 2013; 61: 47–56.
87. Chu PK, Li L. Characterization of amorphous and nanocrystalline carbon films. *Mater Chem Phys* 2006; 96: 253–277.
88. Hui KS, Hui KN, Dinh DA et al. Green synthesis of dimension- controlled Silver nanoparticle-graphene oxide with in situ ultrasonication. *Acta Mater* 2014; 64: 326–332.
89. Shao W, X XL, Min H et al. Preparation, characterization, and antibacterial activity of silver nanoparticle-decorated graphene oxide nanocomposite. *ACS Appl Mater Interfaces* 2015; 7: 6966–6973.

90. de Faria AF, Martinez DST, Meira SMM, de Moraes ACM, Brandelli A, Filho AGS, Alves OL. Anti-adhesion and antibacterial activity of silver nanoparticles supported on graphene oxide sheets. *Colloids Surf B* 2014; 113: 115–124.
91. Gupta A, Chen G, Joshi P et al. Raman Scattering from high-frequency phonons in supported n-graphene layer films. *Nano Lett* 2006; 6: 2667–2673.
92. Neto AHC, Guinea F, Peres NMR et al. The electronic properties of graphene. *Rev Mod Phys* 2009; 8: 109–162.
93. Shearer CJ, Slattery AD, Stapleton AJ et al. Accurate thickness measurement of graphene. *Nanotechnology* 2016; 27: 125704.
94. Graf D, Molitor F, Ensslin K et al. Spatially resolved Raman Spectroscopy of single- and few-layer graphene. *Nano Lett* 2007; 7: 238–242.
95. Lin J, Wang L, Chen G. Modification of graphene platelets and their tribological properties as a lubricant additive. *Tribol Lett* 2011; 41: 209–215.
96. Jiang T, Zhu Y. Measuring graphene adhesion using atomic force microscopy with a microsphere tip. *Nanoscale* 2015; 7: 10760–10766.
97. Zhao G, Li X, Huang M et al. The physics and chemistry of graphene-on-surfaces. *Chem Soc Rev* 2017; 46: 4417–4449.
98. Georgakilas V, Tiwari JN, Kemp KC et al. Noncovalent functionalization of graphene and graphene oxide for energy materials, biosensing, catalytic, and biomedical applications. *Chem Rev* 2016; 116: 5464–5519.
99. Kozlov SM, Viñes F, Görling A. Bonding mechanisms of graphene on metal surfaces. *J Phys Chem C* 2012; 116: 7360–7366.
100. Das S, Lahiri D, Lee DY et al. Measurements of the adhesion energy of graphene to metallic substrates. *Carbon* 2013; 59: 121–129.
101. Preobrajenski AB, Ng ML, Vinogradov AS, Mårtensson N. Controlling graphene corrugation on lattice-mismatched substrates. *Phys Rev B Condens Matter* 2008; 78: 073401.
102. Batzill M. The surface science of graphene: Metal interfaces, CVD synthesis, nanoribbons, chemical modifications, and defects. *Surf Sci Rep* 2012; 67: 83–115.

103. Abbas R, Elkhoshkhany N, Hefnawy A et al. High Stability Performance of Superhydrophobic Modified Fluorinated Graphene Films on Copper Alloy Substrates. *Adv Mater Sci Eng* 2017; 2017: 6197872.
104. Kinoshita H, Nishina Y, Alias AA, Fujii M. Tribological properties of monolayer graphene oxide sheets as water-based lubricant additives. *Carbon* 2014; 66: 720–723.
105. Berman D, Erdemir A, Sumant A. Few layer graphene to reduce wear and friction on sliding steel surfaces. *Carbon* 2013; 54: 454–459.
106. Hanawa T. Research and development of metals for medical devices based on clinical needs. *Sci Technol Adv Mater* 2012; 13: 1–15.
107. De Jesús C, Cruz GJ, Olayo MG, Gómez LM, López-Gracia OG, García-Rosales G, Ramírez-Santiago A, Ríos LC. Coatings by plasmas of pyrrole on nitinol and stainless steel substrates. *Superficies y Vacío* 2012; 25: 157–160.
108. Torabi M, Sadrnezhad SK. Corrosion behavior of polypyrrole/hydroxyapatite nanocomposite thin films electropolymerized on NiTi substrates in simulated body fluid. *Mater Corros* 2011; 62: 252–257.
109. Tepe G, Schmehl J, Wendel HP et al. Reduced thrombogenicity of nitinol stents—In vitro evaluation of different surface modifications and coatings. *Biomaterials* 2006; 27: 643–650.
110. Bhattacharyya A, Dervishi E, Berry B et al. Energy efficient graphite–polyurethane electrically conductive coatings for thermally actuated smart materials. *Smart Mater Struct* 2006; 15: 1–9.
111. Boccaccini AR, Peters C, Roether JA et al. Electrophoretic deposition of polyetheretherketone (PEEK) and PEEK/Bioglass® coatings on NiTi shape memory alloy wires. *J Mater Sci* 2006; 41: 8152–8159.
112. Anjum SS, Rao J, Nicholls JR. Polymer (PTFE) and shape memory alloy (NiTi) intercalated nano-biocomposites. *Mater Sci Eng* 2012; 40: 1–7.
113. Cho J-Y, Ko Y-M, Choe H-C, Brantley WA. Effect of Polymer Coating on the Corrosion Characteristics of Nickel-Titanium Orthodontic Archwire. *Korean J Dent Mater* 2013; 40: 129–136.

114. Yang M-R, Wu SK. DC plasma-polymerized hexamethyldisilazane coatings of an equiatomic TiNi shape memory alloy. *Surf Coat Technol* 2000; 127: 274–281.
115. Carroll WM, Rochev Y, Clarke B et al. Influence of Nitinol wire surface preparation procedures, on cell surface interactions and polymer coating adherence. In *Materials and Processes for Medical Devices Conference*. Anaheim, CA: ASM International 2003; 63–68.
116. Li P, Li L, Wang W et al. Enhanced corrosion resistance and hemocompatibility of biomedical NiTi alloy by atmospheric-pressure plasma polymerized fluorine-rich coating. *Appl Surf Sci* 2014; 297: 109–115.
117. Raza MA, Rehman ZU, Ghauri FA et al. Corrosion study of electrophoretically deposited graphene oxide coatings on copper metal. *Thin Solid Films* 2016; 620: 150–159.
118. Prasai D, Tuberquia JC, Harl RR et al. Graphene: corrosion-inhibiting coating. *ACS Nano* 2012; 6: 1102–1108.
119. Raman RKS, Banerjee PC, Lobo DE et al. Protecting copper from electrochemical degradation by graphene coating. *Carbon* 2012; 50: 4040–4045.
120. Liao Y, Pourzal R, Wimmer MA et al. Graphitic tribological layers in metal-on-metal hip replacements. *Science* 2011; 334: 1687–1690.
121. Lin L-Y, Kim D-E, Kim W-K, Jun S-C. Friction and wear characteristics of multi-layer graphene films investigated by atomic force microscopy. *Surf Coat Technol* 2011; 205: 4864–4869.
122. Liang H, Bu Y, Zhang J et al. Graphene Oxide Film as Solid Lubricant. *ACS Appl Mater Interfaces* 2013; 5: 6369–6375.
123. Buckley F, Hope G. Electroless Deposition of Ag Thin Films. In *International Conference on Nanoscience and Nanotechnology*. Brisbane, Australia: Institute of Electrical and Electronics Engineers 2006; 528–531.
124. Naor H, Avnir D. Electroless Functionalization of Silver Films by Its Molecular Doping. *ACS Appl Mater Interfaces* 2015; 7: 26461–26469.
125. Cheng C, Arunagiri T, Chyan O. Electrodeposition of Silver and Copper/Silver Multilayer on Ruthenium Substrate as a Potential New Metal Interconnect for Integrated Circuits. *Am J Undergrad Res* 2003; 2: 11–18.

126. Byeon JH, Kim J-W. Fabrication of a Pure, Uniform Electroless Silver Film Using Ultrafine Silver Aerosol Particles. *Langmuir* 2010; 26: 11928–11933.
127. Khun NW, Zhang H, Lim LH, Yang J. Mechanical and tribological properties of graphene modified epoxy composites. *KMUTNB Int J Appl Sci Technol* 2015; 8: 101–109.
128. Gurunathan S, Han JW, Park JH et al. Reduced graphene oxide–silver nanoparticle nanocomposite: a potential anticancer nanotherapy. *Int J Nanomedicine* 2015; 10: 6257–6276.
129. Tran M-H, Jeong HK. Synthesis and characterization of silver nanoparticles doped reduced graphene oxide. *Chem Phys Lett* 2015; 630: 80–85.
130. Lee PC, Meisel D. Adsorption and Surface – Enhanced Raman of Dyes on Silver and Gold Sols. *J Phys Chem* 1982; 86: 3391–3395.
131. Poon RWY, Yeung KWK, Liu XY et al. Carbon plasma immersion ion implantation of nickel–titanium shape memory alloys. *Biomaterials* 2005; 26: 2265–2272.
132. Jettanacheawchankit S, Sasithanasate S, Sangvanich P et al. Acemannan stimulates gingival fibroblast proliferation; expressions of keratinocyte growth factor-1, vascular endothelial growth factor, and type I collagen; and wound healing. *J Pharmacol Sci* 2009; 109: 525–531.
133. Mosmann T. Rapid colorimetric assay for cellular growth and survival: application to proliferation and cytotoxicity assays. *J Immunol Methods* 1983; 65: 55–63.
134. Park JH, Park JM. Electrophoretic deposition of graphene oxide on mild carbon steel for anti-corrosion application. *Surf Coat Technol* 2014; 254: 167–174.
135. Dennison JR, Holtz M, Swain G. Raman Spectroscopy of Carbon Materials. *Spectroscopy* 1996; 11: 38–45.
136. Ferrari AC, Robertson J. Origin of the 1150 cm<sup>-1</sup> Raman mode in nanocrystalline diamond. *Phys Rev B* 2001; 63: 1–4.
137. Robertson J. Diamond-like amorphous carbon. *Mater Sci Eng R Rep* 2002; 37: 129–281.
138. Vi TTT, Kumar SR, Rout B et al. The Preparation of Graphene Oxide-Silver Nanocomposites: the Effect of Silver Loads on Gram-Positive and Gram-Negative Antibacterial Activities. *Nanomaterials (Basel)* 2018; 8: 163.



139. Jankovic A, Erakovic S, Vukasinovic-Sekulic M et al. Graphene-based antibacterial composite coatings electrodeposited on titanium for biomedical applications. *Prog Org Coat* 2015; 83: 1–10.
140. Takadoum J, Bennani HH. Influence of substrate roughness and coating thickness on adhesion, friction and wear of TiN films. *Surf Coat Technol* 1997; 96: 272–282.
141. Ding YH, Zhang P, Ren HM et al. Surface adhesion properties of graphene and graphene oxide studied by colloid-probe atomic force microscopy. *Appl Surf Sci* 2011; 258: 1077–1081.
142. Thomas B, Boccaccini A, Shaffer M. Multi-walled carbon nanotube coatings using electrophoretic deposition (EPD). *J Am Ceram Soc* 2005; 88: 980–982.
143. Bragg WH. *An Introduction to Crystal Analysis*. Bell, London: 1928.
144. Liao KH, Lin YS, Christopher WM, Haynes CL. Cytotoxicity of graphene oxide and graphene in human erythrocytes and skin fibroblasts. *ACS Appl Mater Interfaces* 2011; 3: 2607–2615.
145. Ciapetti G, Cenni E, Pratelli L, Pizzoferrato A. In vitro evaluation of cell/biomaterial interaction by MTT assay. *Biomaterials* 1993; 14: 359–364.
146. Sylvester PW. Optimization of the tetrazolium dye (MTT) colorimetric assay for cellular growth and viability. *Methods Mol Biol* 2011; 716: 157–168.
147. Fotakis G, Timbrell JA. In vitro cytotoxicity assays: comparison of LDH, neutral red, MTT and protein assay in hepatoma cell lines following exposure to cadmium chloride. *Toxicol Lett* 2006; 160: 171–177.
148. Cheng C, Nie S, Li S et al. Biopolymer functionalized reduced graphene oxide with enhanced biocompatibility via mussel inspired coatings/anchors. *J Mater Chem B* 2013; 1: 265–275.
149. Suarez-Martinez I, Felten A, Pireaux JJ et al. Transition metal deposition on graphene and carbon nanotubes. *J Nanosci Nanotechnol* 2009; 9: 6171–61715.
150. Zólyomi V, Rusznyák Á, Koltai J et al. Functionalization of graphene with transition metals. *Phys Status Solidi B* 2010; 247: 2920–2923.

151. Liu L, Liu J, Wang Y et al. Facile synthesis of monodispersed silver nanoparticles on graphene oxide sheets with enhanced antibacterial activity. *New J Chem* 2011; 35: 1418–1423.



## VITA

<b>NAME</b>	Dinesh Rokaya
<b>DATE OF BIRTH</b>	30 October 1986
<b>PLACE OF BIRTH</b>	Simikot
<b>INSTITUTIONS ATTENDED</b>	Tribhuvan University Mahidol University
<b>HOME ADDRESS</b>	Simikot-3, Humla District, Karnali Province, Nepal
<b>PUBLICATION</b>	<ol style="list-style-type: none"><li>1. Rokaya D, Srimaneepong V, Qin J, Thunyakitpisal P, Sirlearmukul K. Surface Adhesion Properties and Cytotoxicity of Graphene Oxide Coatings and Graphene Oxide/Silver Nanocomposite Coatings on Biomedical NiTi Alloy. <i>Sci Adv mater</i> 2019 (In Press).</li><li>2. Rokaya D, Srimaneepong V, Sapkota J, Qin J, Sirlearmukul K, Siriwongrungson V. Graphene oxide/Silver nanoparticles coating produced by electrophoretic deposition improved the mechanical and tribological properties of NiTi alloy for biomedical applications. <i>J Nanosci Nanotechnol</i> 2019;19:3804–3810.</li><li>3. Rokaya D, Srimaneepong V, Sapkota J, Qin J, Sirlearmukul K, Vilailuck Siriwongrungson V. An Overview of Polymeric Materials and Films in Dentistry. <i>J Adv Res</i> 2018;14:25-34.</li></ol>
<b>AWARD RECEIVED</b>	The Dean's List Award for Outstanding Student, Faculty of Dentistry, Mahidol University for Academic Year 2014.  The 100th Anniversary Chulalongkorn University for Doctoral Scholarship 2015.



จุฬาลงกรณ์มหาวิทยาลัย  
**CHULALONGKORN UNIVERSITY**